

Nonparanormal Bayesian Dynamic Conditional Partial Correlation Model with Multivariate Volatility Applications*

Hayun Song[†]

This version: October 12, 2023

Abstract

This paper addresses a gap in the limitations of traditional multivariate volatility models in capturing complex conditional dependencies. To address this, we introduce a new perspective through a dynamic framework integrated with the Nonparanormal model for estimating dynamic conditional partial correlations. Unlike existing methodologies, our approach employs precision matrices and focuses on their temporal evolution, providing a more nuanced understanding of conditional independence among multiple assets. The paper makes two contributions. Firstly, it presents a dynamic conditional framework that leverages precision matrices, achieved through Bayesian estimation methods incorporating elements from DCC-GARCH and DC-MSV models. Secondly, the paper handles high-dimensional settings through a coherent Bayesian estimation procedure, addressing the computational burdens associated with large datasets. A Monte Carlo simulation and empirical applications substantiate the method's efficacy, particularly in settings with dynamic conditional correlations. The proposed methodology enhances the granularity of financial market analysis by providing a richer representation of conditional partial correlations over time. This work connects the existing literature across high-dimensional multivariate volatility models, copula models, and Nonparanormal models.

Keywords: High-dimensional multivariate volatility, Bayesian estimation, Structural learning, Dynamic conditional partial correlation

JEL Classification Codes: C11, C32, C58

*I am especially grateful to my adviser Hashem Pesaran for his continuous advice and support. All mistakes are my own.

[†]Department Economics, University of Southern California, Ph.D. Candidate; Correspondence: hayunson@usc.edu.

1 Introduction

Volatility modeling provides important foundations in financial econometrics. While early research predominantly focused on univariate volatility models such as ARCH ([Engle \(1982\)](#)) and GARCH ([Bollerslev \(1986\)](#)), the increasing complexity of financial markets and the advent of high-frequency, high-dimensional data have steered the focus toward multivariate volatility models. These multivariate models capture the dynamic correlations and covariances among multiple assets, thereby providing a more comprehensive framework for understanding market behaviors.

While effective in co-movement respects, these methods may not fully capture the intricate dependencies present in financial returns, particularly when the data exhibit non-normal characteristics such as asymmetry ([Chen, Gerlach, and So \(2006\)](#); [Chiang, Chen, and So \(2007\)](#); [Asai and McAleer \(2011\)](#)) and leptokurtosis ([Wagner and Marsh \(2005\)](#); [So, Chen, Lee, and Chang \(2008\)](#); [Nakajima and Omori \(2012\)](#)). The existing literature has made significant strides in addressing non-normality in relation to volatility, but the question of conditional independence has received less attention. This paper seeks to contribute to the ongoing discourse by proposing an approach that integrates the dynamic framework with the Nonparanormal (semiparametric Gaussian copula) model to estimate dynamic conditional partial correlations. Unlike conditional correlations, conditional partial correlations provide a means to explore direct relationships between variable pairs while taking into account the influence of other interconnected variables. This method recognizes the limitation that conditional independence cannot be readily derived from the simple inversion of conditional covariance. The integration proposed in this paper aims to extend our understanding of asset dependencies and market structures. The method enhances the granularity of financial market analysis by distinguishing the potential influences, offering a more nuanced framework for studying conditional relationships between economic variables.

We make two main contributions. The first contribution entails the introduction of a dynamic conditional framework for assessing volatility by employing precision matrices. Distinctively, our methodology diverges from traditional models such as the Multivariate GARCH (MGARCH) ([Bollerslev \(1990\)](#); [Engle and Kroner \(1995\)](#); [Tse and Tsui \(2002\)](#)) and Multivariate Stochastic Volatility (MSV) ([Harvey, Ruiz, and Shephard \(1994\)](#); [Harvey and Shephard \(1996\)](#); [Kawakatsu \(2006\)](#); [Asai and McAleer \(2009\)](#); [Ishihara, Omori, and Asai \(2016\)](#)) models in two significant ways. Initially, we focus on the temporal evolution of precision matrices, denoted as \mathbf{P}_t , rather than on covariance or correlation matrices. This necessitates the estimation of both the unconditional precision matrix $\boldsymbol{\Omega}$ and the lagged precision matrix $\boldsymbol{\Xi}_{t-1}$. Our primary objective lies in obtaining the conditional partial correlation matrices $\boldsymbol{\Psi}_t$, which encapsulate information on conditional independence. Subsequently, our dynamic framework adopts elements from the Dynamic Conditional Correlation GARCH (DCC-GARCH; [Engle](#)

(2002)) model while assimilating the sampling methodology for Ξ_{t-1} akin to the Dynamic Correlation MSV (DC-MSV; Aas, Czado, Frigessi, and Bakken (2009)) model. Specifically, we sample Ξ_{t-1} from a conjugate Wishart distribution in the posterior distribution. The idea of this framework is that our model synthesizes the strengths of both DCC-GARCH and DC-MSV approaches, capturing the adaptability of GARCH models to incoming data while benefiting from the Bayesian updating mechanism inherent in MSV models for estimating Ξ_{t-1} . This integrative approach allows us to incorporate more complex dynamics into the precision matrices, thereby offering a richer representation of conditional partial correlations over time through the employment of Nonparanormal method (Liu, Lafferty, and Wasserman (2009); Liu, Han, Yuan, Lafferty, and Wasserman (2012)).

Specifically, we follow the Bayesian Nonparanormal approach (Mulgrave and Ghosal (2020, 2022)) to transform the unknown distributions into the approximated normal distribution and construct the rank likelihood (Hoff (2007); Mulgrave and Ghosal (2023)) to construct the sparse precision matrices. Within the DCC framework, the estimation process encompasses two primary components: the univariate GARCH process for predicting variable volatility, and the correlation estimation derived from residuals standardized by the estimated variance from the GARCH process. In the first component, we utilize the t -distribution to enhance the better fit to observed variances. While the t -distribution may indirectly refine correlation estimates by enhancing the fit of marginal distributions via more accurate standardized residuals, the general unknown nature of error distributions and unclear effects on the inverse of the correlation present limitations. It is thereby feasible to employ the nonparanormal method to transform observations into rank-order in the second component. This transformation preserves inter-variable relationships without necessitating specific distributional assumptions. While correct variance estimation retains importance for residual scaling, the construction of rank-likelihood through the nonparanormal model can mitigate the impact of variance estimation errors.

As a second contribution, we offer a coherent Bayesian estimation procedure for dynamic conditional precision matrices to learn the structure of the conditional dependence under high-dimensional settings. We estimate the proposed model using the Bayesian estimation using the Metropolis-Hastings within Gibbs sampling algorithm. One of the goals here is to handle a high-dimensional situation. The DCC-MGARCH type models have been successful in dealing with cases where the number of assets is moderate, for example, less than 25. However, estimation becomes computationally burdensome for large datasets. Similarly, the source of the issue lies in the reliance on an estimation of the unconditional precision matrix, Ω in our proposed model. Given a dataset with T observable time periods and N assets, if the sample covariance matrix is used, it requires to estimate $N(N - 1)/2$ parameters. Hence, without having enough $T \gg N$, it will be subject to significant estimation error. We obtain the precision matrix Ω by sampling the Cholesky decomposable form $\Omega = \mathbf{L}\mathbf{L}'$, where \mathbf{L} is a lower triangular matrix and employ

a horseshoe prior, as delineated in [Neville, Ormerod, and Wand \(2014\)](#) to impose the sparsity. We also utilize the block-updates in the proposal distributions to improve the efficiency of the computation but there is a trade-off with the accuracy.

We illustrate the numerical properties of the method with a Monte Carlo simulation and empirical applications to scrutinize the complexities of financial markets. The simulation involves two designs based on sparse MGARCH models: constant conditional correlations (CCC) and dynamic conditional correlations (DCC), formulated to include sparse and dense elements in the precision matrix. We run 100 replications over varying dimensions N and time periods T , utilizing Gibbs sampling for estimation. The performance of the proposed Nonparanormal Partial Correlation (NPC) method is compared against the Composite Nonlinear Shrinkage (CNLS) approach using Root Mean Square Error (RMSE) metrics between estimated and true inverse correlation matrices. The results suggest that both methods perform suboptimally under CCC but are more effective in DCC settings. Specifically, NPC excels in small sample scenarios, whereas CNLS outperforms NPC when the sample size is large. Distributional assumptions concerning Gaussian versus t-distributions have minimal impact. Complementing the simulation, we empirically investigate time-series data on international stock price indices, S&P 100 stock prices, and foreign exchange rates using standard Wishart and conjugate Wishart priors for precision matrices. We introduce dynamic conditional partial correlations to offer nuanced insights into financial dependencies. The findings reveal the influence of global events and company-specific determinants, enhancing our understanding of the intricate financial landscape.

Our paper extends the existing literature in the areas of high-dimensional multivariate volatility models, copula models, and Nonparanormal models. Within the domain of high-dimensional multivariate volatility models, seminal works by [Ledoit and Wolf \(2003, 2004a,b\)](#) introduced linear shrinkage techniques for optimal covariance matrix estimation, effectively mitigating error maximization by amalgamating sample covariance matrices with structured estimators. Subsequent studies have further refined these methods, introducing non-linear shrinkage (NLS) as a robust mechanism for portfolio optimization ([Ledoit and Wolf \(2012, 2017, 2020, 2022\)](#); [Engle, Ledoit, and Wolf \(2019\)](#); [Nard, Engle, Ledoit, and Wolf \(2022\)](#)). The extension of these models to accommodate dynamic settings through DCC frameworks has been explored by [Engle, Ledoit, and Wolf \(2019\)](#) and [Pakel, Shephard, Sheppard, and Engle \(2021\)](#). In contrast, within the literature advocating sparsity-based approaches, [Bickel and Levina \(2008a,b\)](#), [Rothman, Levina, and Zhu \(2009\)](#), and [Cai and Liu \(2011\)](#) have proposed methodologies for banding and thresholding covariance matrices based on variable ordering. [Chen and Leng \(2016\)](#) devised a class of dynamic covariance models (DCMs), employing kernel smoothing and subsequent entry-wise thresholding on the locally estimated matrices. Further extensions to semiparametric approaches involving diverging conditioning variables have

been explored by [Chen, Li, and Linton \(2019\)](#). Moreover, [Poignard and Asai \(2023\)](#) ventured into high-dimensional variance-covariance matrix modeling within the Multivariate Stochastic Volatility (MSV) framework, sidestepping the need for Monte Carlo methods by leveraging Vector Autoregressive and Moving-Average (VARMA) representations. Notably, our methodology aligns with the sparsity-based frameworks, specifically focusing on the structure learning of dynamic conditional precision matrices—an aspect conspicuously underrepresented in the aforementioned literature.

In the realm of financial econometrics, traditional multivariate volatility models have long served as a cornerstone for capturing linear dependencies and facilitating dimensionality reduction. Nevertheless, these models exhibit a circumscribed ability to encapsulate non-linear and tail dependencies, thereby necessitating more sophisticated modeling techniques. The application of copula methods has become prominent as a versatile framework for capturing a diverse range of dependency structures, encompassing both linear and tail dependencies ([Patton \(2009\)](#); [Aas, Czado, Frigessi, and Bakken \(2009\)](#); [Anatolyev and Pyrlik \(2022\)](#)). Subsequent advancements in the domain have yielded specific models such as Pair Copula Constructions (PCC) ([Müller and Czado \(2019a\)](#)), vine copulas ([Müller and Czado \(2019b\)](#)), and Gaussian Copula Graphical Models (GCGM) ([Pitt, Chan, and Kohn \(2006\)](#); [Dobra and Lenkoski \(2011\)](#); [Liu, Han, Yuan, Lafferty, and Wasserman \(2012\)](#); [Mohammadi, Abegaz, Heuvel, and Wit \(2017\)](#)). These specialized models facilitate the scrutiny of ultra-high-dimensional data with complex interdependencies. Furthermore, the utility of copula methods has been expanded to accommodate dynamic dependencies through the incorporation of DCC frameworks ([Kim and Jung \(2016\)](#); [Oh and Patton \(2016, 2017, 2023\)](#)). However, despite their versatility, copula models often presuppose rigid functional forms for dependencies, which may misalign with empirical phenomena. To mitigate this, the Nonparanormal model was introduced as a semiparametric enhancement of Gaussian graphical models, endowed with the capability to capture non-Gaussian marginal distributions through smooth, monotonic transformations ([Liu, Lafferty, and Wasserman \(2009\)](#)). Subsequent developments in this line of inquiry have addressed high-dimensional settings in Bayesian Nonparanormal graphical model ([Mulgrave and Ghosal \(2020, 2022, 2023\)](#)). Building on this foundation, our research contributes a novel methodological framework inspired by Nonparanormal models. Distinctively, our approach accounts for the dynamic and conditional nature of precision matrices—an aspect conspicuously underexplored in extant literature. While our model employs a rank likelihood methodology analogous to certain copula models, it remains fundamentally grounded in the Nonparanormal paradigm. A feature of our approach is the estimation of partial correlation matrices, thereby diverging from existing DCC-based models that predominantly focus on full correlation matrices.

More broadly, we connect to the literature that focuses on quantifying interconnectedness through various lenses: measure-based approaches ([Billio, Getmansky, Lo, and Pelizzon \(2012\)](#);

Diebold and Yilmaz (2015); Hautsch, Schaumburg, and Schienle (2015); Härdle, Wang, and Yu (2016)), vector autoregressions (VAR) (Dahlhaus (2000); Eichler (2007); Diebold and Yilmaz (2014); Baruník and Křehlík (2018); Barigozzi and Brownlees (2019); Bykhovskaya (2022)), and factor structures in adjacency matrices (Barigozzi, Cavalieri, and Moramarco (2022)). While much of the extant literature explores the integration of VARs into network models, recent research by Mlikota (2022) reverses this focus, investigating the incorporation of networks into VAR frameworks.

The remainder of the paper is structured as follows. Section 2 delineates the underlying econometric framework, subdivided into several key components. Section 2.1 formalizes the architecture of the Dynamic Conditional Partial Correlation framework. Section 2.2 elaborates on rank transformation and likelihood within a Bayesian context. Section 2.3 focuses on the implementation of Gibbs sampling for estimating a sparse unconditional precision matrix (Ω). Section 2.4 explores the Bayesian estimation applied to the GARCH process within the proposed Dynamic Conditional Partial Correlation framework. Section 3 presents simulation outcomes for the introduced estimators. Section 4 employs the estimation framework across three empirical domains: section 4.1 focuses on foreign stock price indices, section 4.2 on domestic stock prices, and section 4.3 on exchange rates. Section 5 offers interpretative insights into the estimators and explores model extensions, including the integration of common factors. The concluding section provides a summary and implications of the research. Supplementary material, encompassing technical nuances and additional empirical visualizations, is relegated to the appendices.

2 Nonparanormal Bayesian Dynamic Conditional Partial Correlation

2.1 Dynamic conditional partial correlation framework

Let $y_{it} = \ln(p_{it}/p_{i,t-1})$ be a financial security i 's return at time t can be defined as the change in logarithmic prices, where p_{it} is a security i 's price at time t and $\mathbf{y}_t = (y_{1t}, y_{2t}, \dots, y_{Nt})$ be the price information up to time t and the set of known information up to time t , \mathcal{F}_t for $t = 1, 2, \dots, T$. The model is defined as

$$\mathbf{y}_t = \boldsymbol{\mu}_t + \mathbf{H}_t^{1/2} \boldsymbol{\epsilon}_t, \quad \text{for } t = 1, \dots, T, \quad (2.1)$$

where $\boldsymbol{\mu}_t = \mathbb{E}(\mathbf{y}_t | \mathcal{F}_{t-1})$, and $\mathbf{H}_t = \{h_{ij,t}\}_{i,j=1}^N = \text{Cov}(\mathbf{y}_t | \mathcal{F}_{t-1})$ is an $N \times N$ positive-definite conditional covariance matrix. The error vectors are i.i.d. with $\mathbb{E}(\boldsymbol{\epsilon}_t | \mathcal{F}_{t-1}) = 0$ and $\mathbb{E}(\boldsymbol{\epsilon}_t \boldsymbol{\epsilon}_t' | \mathcal{F}_{t-1}) = \mathbb{I}_N$, where \mathbb{I}_N is the identity matrix of order N if the the conditional mean and covariance matrix

are correctly specified. Following the framework in MGARCH model, \mathbf{H}_t is expressed as

$$\mathbf{H}_t = \mathbf{D}_t^{1/2} \mathbf{S}_t^{-1} \mathbf{D}_t^{1/2}, \quad (2.2)$$

where $\mathbf{D}_t^{1/2} = \text{diag}\{\mathbf{H}_t^{1/2}\} = \text{diag}\{h_{1,t}^{1/2}, \dots, h_{N,t}^{1/2}\}$, and each conditional variance is specified as a GARCH(1,1) model

$$h_{it} = w_i + \theta_{0,i} r_{i,t-1}^2 + \theta_{1,i} h_{i,t-1}, \quad (2.3)$$

where $(w_i, \theta_{0,i}, \theta_{1,i})$ are the variable-specific GARCH(1,1) parameters with $w_i > 0$, $\theta_{0,i} \geq 0$, $\theta_{1,i} \geq 0$, $\theta_{0,i} + \theta_{1,i} < 1$, $i = 1, \dots, N$, $r_{it} = y_{it} - \mu_t$, and \mathbf{S}_t is an inverse correlation matrix.

It is noteworthy that our analytical framework adopts the GARCH(1,1) specification, a choice consciously made despite its inherent constraints. Specifically, the model imposes positivity restrictions on its parameters to assure positive conditional variance and relies on a summation of squared past residuals, as delineated in Equation (2.3). These characteristics engender limitations such as short-term memory and symmetric volatility response. Additionally, the model faces challenges in capturing long-term positive serial correlation owing to the exponential decay of the influence of past squared returns.

While these constraints could be circumvented through alternative specifications—such as Exponential GARCH (EGARCH; [Nelson \(1991\)](#)), Quadratic GARCH (QGARCH; [Sentana \(1995\)](#)), Threshold GARCH ([Chen and So \(2006\)](#); [Chen, Liu, and So \(2008\)](#)), or Fractionally Integrated GARCH (FIGARCH; [Baillie, Bollerslev, and Mikkelsen \(1996\)](#))—our primary focus remains on the dependency structures constructed. In line with this, our methodology incorporates a Bayesian estimation approach, accommodating skewed and heavy-tailed error distributions. Specifically, we employ a multivariate t -distribution characterized by ν degrees of freedom for error terms, as suggested by [Fioruci, Ehlers, and Andrade Filho \(2014\)](#).

The inverse correlation matrix, $\mathbf{S}_t = \{s_{ij,t}\}_{i,j=1}^N$, is formulated as

$$\mathbf{S}_t = \text{diag}\{\mathbf{P}_t\}^{-1/2} \mathbf{P}_t \text{diag}\{\mathbf{P}_t\}^{-1/2},$$

where \mathbf{P}_t denotes an $N \times N$ symmetric, positive-definite conditional precision matrix of the transformed devolatilized residuals \mathbf{z}_t . These transformed residuals are derived from the raw devolatilized residuals, represented as $\mathbf{u}_t = \mathbf{D}_t^{-1}(\mathbf{y}_t - \boldsymbol{\mu}_t)$, with the aim of approximating a Gaussian distribution. Specifically, the matrix $\mathbf{U} = (\mathbf{u}_1, \mathbf{u}_2, \dots, \mathbf{u}_T)'$ is transformed into $\mathbf{Z} = (\mathbf{z}_1, \mathbf{z}_2, \dots, \mathbf{z}_T)' \sim \mathcal{N}(\mathbf{0}, \mathbf{S}^{-1})$, where $\mathbf{S} = \text{diag}\{\boldsymbol{\Omega}\}^{-1/2} \boldsymbol{\Omega} \text{diag}\{\boldsymbol{\Omega}\}^{-1/2}$ via a Nonparanormal transformation facilitated by Gibbs sampling. The core objective of this transformation is to approximate normality for the standardized residuals, thereby imbuing the resultant partial correlation matrices with meaningful interpretability concerning conditional independence—a focal point of our exploration into volatility dependence in this paper.

The evolution of the conditional precision matrix over time is governed by the following specification

$$\mathbf{P}_t = (1 - a - b) \boldsymbol{\Omega} + a \boldsymbol{\Xi}_{t-1} + b \mathbf{P}_{t-1}, \quad (2.4)$$

where (a, b) are the parameters with $a > 0$, $b > 0$ and $a + b < 1$. The unconditional precision matrix, $\boldsymbol{\Omega}$, is sampled from the Gibbs sampling with horseshoe priors and the lagged synchronization precision matrix, $\boldsymbol{\Xi}_{t-1}$, is drawn from a conjugate posterior Wishart distribution

$$\boldsymbol{\Xi}_{t-1} \sim \mathcal{W}(T + 3, (\mathbb{I}_n + \mathbf{z}_{t-1} \mathbf{z}'_{t-1})^{-1}) \quad (2.5)$$

facilitating the generation of a precision sample dependent on the transformed devolatilized residuals. The conjugacy with the normal distribution of \mathbf{z}_t , as yielded by the nonparanormal transformation, permits closed-form expression for the posterior. The Wishart distribution, a probability distribution over symmetric positive-definite matrices, inherently captures the structure and dependencies in the data. Its parameters eliminate the need for additional constraints or regularization, ensuring that the sampled matrices are positive definite and align with the underlying structure of the data.

Our proposed model for the temporal evolution of conditional precision matrices, denoted as \mathbf{P}_t , finds its theoretical underpinnings in both the Multivariate GARCH (MGARCH) and Multivariate Stochastic Volatility (MSV) frameworks. Analogous to the DCC–MGARCH model ([Engle \(2002\)](#)), \mathbf{P}_t serves as the conditional precision of \mathbf{z}_t conditional on \mathcal{F}_{t-1} . Employing sampled $\boldsymbol{\Omega}$ values allows us to derive the time-varying inverse correlation matrix, \mathbf{S}_t . However, our model distinguishes itself by considering $\boldsymbol{\Xi}_{t-1}$ as a function of lagged transformed standardized residuals, akin to the VC–MGARCH model ([Tse and Tsui \(2002\)](#)). Rather than treating $\boldsymbol{\Xi}_{t-1}$ as a stochastic variable as in the DC–MSV model ([Asai and McAleer \(2009\)](#)), we sample it from a Wishart distribution with pre-defined hyperparameters, as specified in Equation (2.5).

Our Bayesian estimation framework incorporates coefficients for both $\boldsymbol{\Omega}$ and $\boldsymbol{\Xi}_{t-1}$, serving as scaling factors that modulate their respective contributions to \mathbf{P}_t . These coefficients enhance model adaptability to potential market structural shifts and enrich interpretability by elucidating the relative importance of each factor in determining conditional independence structures. Exclusion of these coefficients, as in conventional MSV models, may offer computational simplicity and increased flexibility but at the expense of interpretive richness.

Furthermore, it is pertinent to acknowledge the contributions of [Billio, Caporin, and Gobbo \(2003\)](#), who argue that varying systems could have differential impacts on current observed values. In this context, the Clustered Correlation MGARCH model (CC–MGARCH; [So and Yip \(2012\)](#)) provides an adjustment to Equation (2.4) to account for this system-specific influence. While this augmentation enhances the model's flexibility, it simultaneously adds to the computational burden due to an expanded parameter set, especially when integrated with

the conditional variance scheme outlined in Equation (2.3). This increased complexity poses challenges for both estimation procedures and interpretive clarity in scenarios involving high-dimensional data.

Given the dynamic conditional inverse correlation matrix \mathbf{S}_t , we can find the dynamic conditional partial correlation matrix $\boldsymbol{\Psi}_t = \{\psi_{ij,t}\}_{i,j=1}^N$ as

$$\psi_{ij,t} = \begin{cases} -s_{ij,t}/\sqrt{s_{ii,t}s_{jj,t}}, & \text{for } i \neq j \\ 1 & \text{for } i = j \end{cases}. \quad (2.6)$$

To interpret the partial correlation matrix within the conditional independence structure, the likelihood from the standardized residuals must follow multivariate Gaussian distributions. This is achieved by applying a nonparanormal transformation of \mathbf{u}_t and using rank likelihood to obtain \mathbf{P}_t from $\boldsymbol{\Omega}$ and $\boldsymbol{\Xi}_{t-1}$. Notably, even though \mathbf{P}_t is unidentifiable in (2.4), we can obtain an identifiable $\boldsymbol{\Psi}_t$ due to the scale invariance of the rank likelihood, thus maintaining the same distribution between non-identifiable and identifiable models.

Remark 1. Recall that the existing MGARCH and MSV models employ a conditional correlation matrix \mathbf{R}_t that evolves based on a predefined set of dynamics involving the conditional covariance matrix \mathbf{Q}_t . A modified framework, which replaces \mathbf{Q}_t with a conditional precision matrix \mathbf{P}_t , yields an alternative conditional correlation matrix \mathbf{S}_t^{-1} . Despite both \mathbf{R}_t and \mathbf{S}_t^{-1} serving as conditional correlation matrices, their divergence arises from the distinct dynamics governing \mathbf{Q}_t and \mathbf{P}_t . Consequently, while the conditional covariance matrices \mathbf{H}_t constructed from these correlation matrices share identical diagonal elements, the off-diagonal elements, representing conditional covariances, differ. Specifically, \mathbf{S}_t^{-1} is likely to focus on the linear dependencies conditional on the other variables in the system, given that precision matrices often provide insights into conditional independence. This can imply that \mathbf{H}_t in this modified framework is better suited for capturing partial correlations or for isolating the unique relationships between each pair of time series after accounting for the influence of other variables.

2.2 Bayesian Rank transformation and likelihood

To infer the unconditional inverse covariance matrix $\boldsymbol{\Omega}$, we commence by transforming the raw standardized residuals $\mathbf{U} = (\mathbf{u}_1, \mathbf{u}_2, \dots, \mathbf{u}_T)' = (\mathbf{U}_1, \mathbf{U}_2, \dots, \mathbf{U}_N)$ into $\mathbf{Z} = (\mathbf{z}_1, \mathbf{z}_2, \dots, \mathbf{z}_T)' = (\mathbf{Z}_1, \mathbf{Z}_2, \dots, \mathbf{Z}_N) \sim \mathcal{N}(\mathbf{0}, \mathbf{C})$, where $\mathbf{C} = \mathbf{S}^{-1}$. Recall that our primary focus is the inference of the unconditional inverse correlation matrices \mathbf{S} since the rank transformation does not retain the original scale or variances. This methodology aligns with the Gibbs sampling approaches proposed by [Mulgrave and Ghosal \(2023\)](#).

We delineate the set $\mathcal{B} = \{\mathbf{Z} \in \mathbb{R}^{T \times n} : u_{i,t_{r-1}} < u_{i,t_r} < u_{i,t_{r+1}}\}$ subject to order constraints, with a rank of the observations $r = 2, \dots, T - 1$. The transformed variables \mathbf{Z} are restricted to

reside within this set. The rank-likelihood $L^{\text{RL}}(\mathbf{Z})$ is then articulated as:

$$L^{\text{RL}}(\mathbf{Z}) = \Pr(\mathbf{Z} \in \mathcal{B} | \mathbf{C}, g_1, \dots, g_n) = \int_{\mathcal{B}} p(\mathbf{Z} | \mathbf{C}) d\mathbf{Z} = \Pr(\mathbf{Z} \in \mathcal{B} | \mathbf{C}),$$

where g_i, \dots, g_p are transformation functions. This likelihood is exclusively contingent on \mathbf{C} , devoid of dependency on specific transformation functions ([Hoff \(2007\)](#)). Utilizing Gibbs sampling as described in Algorithm 1, Appendix, we derive the posterior distribution

$$\Pr(\mathbf{S} | \mathbf{Z} \in \mathcal{B}) \propto p(\mathbf{S}) p(\mathbf{Z} \in \mathcal{B} | \mathbf{S}).$$

Specifically, the algorithm traverses each of n variables across T time points, setting boundary values for each observation based on its neighbors. It then calculates a conditional mean and variance for each observation using predefined covariate matrices and samples from a truncated normal distribution within the established boundaries. This approach provides an efficacious means to capture the underlying correlation structure without the necessity of explicit distributional assumptions regarding the transformation functions.

This rank-based Nonparanormal approach presents a deviation from both the Copula and the standard Nonparanormal frameworks. The Copula model mandates a two-step transformations. Initially, \mathbf{U}_i are transformed into the uniform margins $\tilde{\mathbf{U}}_i$ via their respective empirical Cumulative Distribution Functions (CDFs), $\tilde{\mathbf{U}}_i = F_i(\mathbf{U}_i) \sim \mathcal{U}(0, 1)$ for $i = 1, \dots, N$. Subsequently, these uniform variables are converted into standard normal margins by employing the inverse standard normal CDF, Φ^{-1} , denoted as $\mathbf{Z}_i = \Phi^{-1}(\tilde{\mathbf{U}}_i)$. Then, the joint likelihood $L^{\text{CP}}(\mathbf{Z})$ in the Gaussian copula model is then constructed as the product of individual marginal likelihoods and the copula density, represented as

$$L^{\text{CP}}(\mathbf{Z}) = \prod_{i=1}^N f(\mathbf{Z}_i) \cdot c(\mathbf{Z}; \mathbf{C}),$$

where $f(\mathbf{Z}_i)$ is the marginal density of \mathbf{Z}_i , $c(\mathbf{Z}; \mathbf{C})$ denotes the copula density, and \mathbf{C} is the correlation matrix capturing the dependencies among the \mathbf{Z}_i 's. The likelihood construction in this approach decomposes into marginal and copula components. Conversely, the Nonparanormal model extends this by introducing smooth, invertible functions to transform the original variables before the copula transformation, leading to a likelihood formulation that additionally involves these transformation functions g_i , resulting in transformed observations $g_i(u_{it})$. The core premise is that these transformed variables approximate a multivariate Gaussian distribution, obviating the need for additional transformations to uniform or standard normal margins. Under this Gaussian assumption, the joint likelihood $L^{\text{NP}}(\mathbf{Z})$ for the transformed dataset \mathbf{Z} ,

where $z_{it} = g_i(u_{it})$, is formulated as

$$L^{\text{NP}}(\mathbf{Z}) = \prod_{i=1}^N \prod_{t=1}^T f(z_{it}) \cdot |J(g_i(u_{it}))|,$$

where $f(z_{it})$ denotes the Gaussian density function for the transformed variables z_{it} and $|J(g_i(u_{it}))|$ is the absolute value of the Jacobian determinant of the transformation g_i at u_{it} . This likelihood construction directly models the dependencies among variables and across time, capitalizing on the Gaussian approximation.

Consequently, the Rank-based Nonparanormal model serves as an intermediary between the Copula and traditional Nonparanormal frameworks. It avoids the Copula model's requisite partitioning of marginal and copula components, thereby streamlining the likelihood formulation. Simultaneously, it circumvents the Nonparanormal model's need for estimating smooth transformation functions h_i , thereby reducing model intricacy. This approach amalgamates the respective merits of both models while attenuating their individual complexities and assumptions.

2.3 Gibbs sampling for sparse unconditional precision matrix

We obtain the sparse unconditional precision matrix $\boldsymbol{\Omega}$ by sampling the Cholesky decomposable form $\boldsymbol{\Omega} = \mathbf{L}\mathbf{L}'$, where \mathbf{L} is a lower triangular matrix. This decomposition facilitates the derivation of the regression framework from the multivariate Gaussian model, following the approach by Rue and Held (2005). Specifically, the lower triangular elements of $\boldsymbol{\Omega}$ are defined as

$$\Omega_{ij} = \sum_{k=1}^j L_{ik} L_{jk} = \sum_{k=1}^j \beta_{ik} \beta_{jk} \omega_k,$$

where $\beta_{ij} = -L_{ij}/L_{jj}$ represents the coefficients, and $\omega_j = 1/\sigma_j^2 = L_{jj}^2$ denotes the precision of the multivariate Gaussian distribution.

By employing the transformed standardized residuals $\mathbf{Z} \sim \mathcal{N}_N(\mathbf{0}, \mathbf{C})$, the regression equation can be formulated as

$$\mathbf{Z}_j = \boldsymbol{\mu}_j + \sum_{i>j} \beta_{ij} (\mathbf{Z}_i - \boldsymbol{\mu}_i) + \boldsymbol{\eta}_j, \quad \boldsymbol{\eta}_j \sim \mathcal{N}(\mathbf{0}, \omega_j^{-1}) \quad (2.7)$$

for $j = 1, 2, \dots, N$ and $i = j+1, j+2, \dots, N$, where $\boldsymbol{\mu}_j$ and $\boldsymbol{\mu}_i$ denote the constant mean vectors corresponding to the variables j and i . This formulation ensures the properties of symmetry and positive definiteness in the precision matrix. Derived from Equation (2.7), the likelihood function takes the form

$$\mathbf{Z}_j | \mathbf{Z}_{i>j}, \boldsymbol{\beta}_{i>j}, \sigma_j^2 \sim \mathcal{N} (\mathbf{Z}_{i>j} \boldsymbol{\beta}_{i>j}, \sigma_j^2 \mathbb{I}), \quad (2.8)$$

where $\mathbf{Z}_{i>j}$ refers to the matrix constructed by the columns of \mathbf{Z} greater than j , and $\boldsymbol{\beta}_{i>j} = (\beta_{j+1,j}, \beta_{j+2,j}, \dots, \beta_{N,j})$.

Recognizing the inherent ordering of variables within the regression model, we apply a sparsity constraint across the rows of the lower triangular matrix, as detailed in [Mulgrave and Ghosal \(2022\)](#). This procedure maintains a consistent probability of nonzero entries across rows, governed by $\frac{c}{n\sqrt{i}}$, with c serving as a tunable parameter. For the regression coefficients β_{ij} , we employ a horseshoe prior, as delineated in [Neville, Ormerod, and Wand \(2014\)](#), with the global scale parameter λ_j approximating the probability of a nonzero element. We employ the horseshoe prior, characterized by its concentration around zero and tails resembling a Cauchy distribution, thereby offering robust variable selection and the ability to capture extreme values. This selection stands in contrast to other commonly used priors such as the Gaussian and Laplace, which are limited by their lighter tails and less effective variable selection capabilities. The spike-and-slab prior ([Li and McCormick \(2019\)](#); [Mulgrave and Ghosal \(2020\)](#)), while designed for inducing sparsity, can be computationally demanding and less apt at modeling fat-tailed distributions. The G-Wishart prior ([Mohammadi and Wit \(2015\)](#); [Mohammadi, Abegaz, Heuvel, and Wit \(2017\)](#)), on the other hand, is tailored for capturing structural sparsity in graph-based models but may not be optimal for handling fat-tailed behavior. Hence, the horseshoe prior provides a balanced and effective approach for modeling the precision matrix's sparsity and tail behavior, attributes that are frequently observed in financial data.

The combined application of sparsity constraints and carefully chosen priors induces a structured prior on $\boldsymbol{\Omega}$, subsequently influencing the prior on \mathbf{S} . For a comprehensive exposition of the sparsity mechanism, refer to [Mulgrave and Ghosal \(2022\)](#). The specific algorithm employed for the implementation is elaborated in Algorithm 2, Appendix.

2.4 Bayesian GARCH Estimation

In line with the DCC framework, the GARCH model yields conditional variances h_{it} for each i and t . The conditional likelihood function, as stipulated in Equation (2.1), is expressed as:

$$\begin{aligned} l(\boldsymbol{\theta} | \mathbf{Y}) &= \prod_{t=1}^T |\mathbf{H}_t|^{-1/2} p_{\epsilon} \left(\mathbf{H}_t^{-1/2} \mathbf{y}_t \right) \\ &= \prod_{t=1}^T \left[\prod_{i=1}^n h_{it}^{-1/2} \right] |\mathbf{S}_t^{-1}|^{-1/2} p_{\epsilon} \left((\mathbf{D}_t \mathbf{S}_t^{-1} \mathbf{D}_t)^{-1/2} \mathbf{y}_t \right), \end{aligned}$$

where p_{ϵ} represents the joint density function for ϵ_t , parameterized by $\{w_1, \theta_{10}, \theta_{11}, \dots, w_N, \theta_{N0}, \theta_{N1}, a, b\}$ in Equations (2.4) and (2.3). We adopt the multivariate skewed distributions characterized by a shape parameter $\gamma > 0$, which quantifies the degree of asymmetry as formulated by Bauwens and Laurent (2005):

$$p_{\epsilon}(\epsilon_t | \gamma) = 2^N \left(\prod_{i=1}^N \frac{\gamma_i \sigma_{\gamma_i}}{1 + \gamma_i^2} \right) \frac{\Gamma((\nu + N)/2)}{\Gamma(\nu/2) [\pi(\nu - 2)]^{N/2}} \left[1 + \frac{\epsilon_t^* \epsilon_t^*}{\nu - 2} \right]^{-\frac{\nu+N}{2}}, \quad (2.9)$$

and

$$\epsilon_t^* = \begin{cases} (\epsilon_t \sigma_{\gamma_i} + \mu_{\gamma_i}) / \gamma_i & \text{if } \epsilon_t \geq -\mu_{\gamma_i} / \sigma_{\gamma_i}, \\ (\epsilon_t \sigma_{\gamma_i} + \mu_{\gamma_i}) \gamma_i & \text{if } \epsilon_t < -\mu_{\gamma_i} / \sigma_{\gamma_i} \end{cases},$$

where $\Gamma(\cdot)$ signifies the Gamma function, μ_{γ_i} and $\sigma_{\gamma_i}^2$ are determined as:

$$\mu_{\gamma_i} = \frac{\Gamma((\nu - 1)/2) \sqrt{\nu - 2} (\gamma - 1/\gamma)}{\sqrt{\pi} \Gamma(\nu/2)},$$

$$\sigma_{\gamma_i}^2 = (\gamma_i^2 + 1/\gamma_i^2) - \mu_{\gamma_i}^2 - 1,$$

and ν is the degree of freedom (tail) parameter. This methodology decouples the influence of skewness and tail characteristics while anchoring the mode at zero. The shape parameter γ governs the distribution of mass on either side of the mode, whereas the tail parameter ν modulates the distribution's skewness. A γ value of 1 engenders symmetric distributions, while $\gamma > 1$ and $\gamma < 1$ are indicative of right and left skewness, respectively. As $\nu \rightarrow \infty$, the distribution converges to a standard multivariate normal distribution, as demonstrated by Fernández and Steel (1998).

In accordance with the GARCH(1,1) model as defined in Equation (2.3), the priors for ω_i , $\theta_{0,i}$, and $\theta_{1,i}$ are drawn from truncated normal distributions, as expressed below for $i = 1, 2, \dots, N$. This formulation is consistent with Ardia (2008):

$$\omega_i \sim \mathcal{N}(\mu_{\omega_i}, \sigma_{\omega_i}^2) I(\omega_i > 0),$$

$$\theta_{0,i} \sim \mathcal{N}(\mu_{\theta_{0i}}, \sigma_{\theta_{0i}}^2) I(0 < \theta_{0,i} < 1),$$

$$\theta_{1,i} \sim \mathcal{N}(\mu_{\theta_{1i}}, \sigma_{\theta_{1i}}^2) I(0 < \theta_{1,i} < 1),$$

where $I(\cdot)$ denotes a indicator function. Analogously, the parameters a and b in Equation (2.4) are drawn from:

$$a \sim \mathcal{N}(\mu_a, \sigma_a^2) I(0 < a < 1), \quad b \sim \mathcal{N}(\mu_b, \sigma_b^2) I(0 < b < 1).$$

For the additional parameters γ_i and ν , the priors are specified as:

$$\gamma_i \sim \mathcal{N}(\mu_{\gamma_i}, \sigma_{\gamma_i}^2) I(\gamma_i > 0), \quad \nu \sim \mathcal{N}(\mu_\nu, \sigma_\nu^2) I(\nu > 2).$$

Refer to Algorithm 3 in Appendix for further algorithmic specifications.

3 Monte Carlo Experiments

We consider the following Monte Carlo simulations. The data generating process (DGP) of the experiment is, for $r = 1, 2, \dots, 100$ simulations,

$$y_{it}^{(r)} = \mu_t^{(r)} + u_{it}^{(r)}, \quad \text{for } i = 1, 2, \dots, N; t = 1, 2, \dots, T,$$

where $\mu_t^{(r)} \stackrel{i.i.d.}{\sim} \mathcal{U}(0.5, 1.5)$. The errors $u_{it}^{(r)}$ are generated as

$$u_{it}^{(r)} = \sqrt{h_{it}^{(r)}} \varepsilon_{it}^{(r)}, \quad \text{for } i = 1, 2, \dots, N; t = -50, -49, \dots, -1, 0, 1, \dots, T-1, T,$$

where $u_{i,-50}^{(r)} = \sqrt{h_{i,-50}^{(r)}} \varepsilon_{i,-50}^{(r)}$, and $h_{i,-50}^{(r)} = \sigma_i^{2,(r)} \stackrel{i.i.d.}{\sim} (\frac{1}{2} + \frac{\chi^2(2)}{4})$. We consider two different distributions for $\varepsilon_{it}^{(r)}$ following

$$\varepsilon_{it}^{(r)} \stackrel{i.i.d.}{\sim} \mathcal{N}(0, 1), \quad \text{and} \quad \varepsilon_{it}^{(r)} \stackrel{i.i.d.}{\sim} \text{scale} \cdot t(\nu = 3),$$

where $\text{scale} = \sqrt{\frac{\nu-2}{\nu}}$ and ν is a degree-of-freedom. We have two simulation designs for $h_{it}^{(r)}$. The first one assumes that the data arises from the sparse multivariate GARCH with the constant conditional correlations (CCC) and the constant sparsity. The second one assumes that the data has been generated by the sparse multivariate GARCH with the dynamic conditional correlations (DCC) and the time-varying sparsity.

As the first simulation setup, we adopt a sparse MGARCH model with CCC framework. Define $\mathbf{h}_t^{(r)}$ and $\mathbf{r}_t^{(r)}$ as

$$\mathbf{h}_t^{(r)} = (h_{1t}^{(r)}, h_{2t}^{(r)}, \dots, h_{Nt}^{(r)})' \quad \text{and} \quad \mathbf{r}_t^{(r)} = (r_{1t}^{(r)}, r_{2t}^{(r)}, \dots, r_{Nt}^{(r)})' = \mathbf{y}_t^{(r)} - \boldsymbol{\mu}_t^{(r)}.$$

The conditional variance $\mathbf{h}_t^{(r)}$ are governed by

$$\mathbf{h}_t^{(r)} = \mathbf{W}^{(r)} + \boldsymbol{\Theta}_0^{(r)} \mathbf{r}_{t-1}^{2,(r)} + \boldsymbol{\Theta}_1^{(r)} \mathbf{h}_{t-1}^{(r)} > 0, \quad (3.1)$$

where $\mathbf{W}^{(r)} = (w_1^{(r)}, w_2^{(r)}, \dots, w_N^{(r)})'$, $w_i^{(r)} = (1 - \theta_{i0}^{(r)} - \theta_{i1}^{(r)}) \sigma_i^{2,(r)}$, $\boldsymbol{\Theta}_0^{(r)} = \text{diag}\{\theta_{10}^{(r)}, \theta_{20}^{(r)}, \dots, \theta_{N0}^{(r)}\}$ and $\boldsymbol{\Theta}_1^{(r)} = \text{diag}\{\theta_{11}^{(r)}, \theta_{21}^{(r)}, \dots, \theta_{N1}^{(r)}\}$. The parameters are sampled from $\theta_{i0}^{(r)} \stackrel{i.i.d.}{\sim} \mathcal{U}(0.1, 0.2)$,

$\theta_{i1}^{(r)} \stackrel{i.i.d.}{\sim} \mathcal{U}(0.5, 0.75)$ and $\sigma_i^{2,(r)} \stackrel{i.i.d.}{\sim} \left(\frac{1}{2} + \frac{\chi^2(2)}{4}\right)$, respectively. For generating $\mathbf{y}_t^{(r)}$, we use

$$\mathbf{y}_t^{(r)} = \boldsymbol{\mu}_t^{(r)} + \left\{ \mathbf{D}_t^{(r)} \right\}^{1/2} \mathbf{L}_{\mathbf{S}}^{-1} \boldsymbol{\varepsilon}_t^{(r)}$$

with $\mathbf{D}_t^{(r)} = \text{diag} \left\{ h_{1t}^{(r)}, h_{2t}^{(r)}, \dots, h_{Nt}^{(r)} \right\}$, $\mathbf{L}_{\mathbf{S}}$ is a Cholesky factor of $\mathbf{S}^{(r)} = \text{diag}\{\boldsymbol{\Omega}^{(r)}\}^{-1/2} \boldsymbol{\Omega}^{(r)} \text{diag}\{\boldsymbol{\Omega}^{(r)}\}^{-1/2}$, and $\boldsymbol{\Omega}^{(r)} = \boldsymbol{\Omega}_{\text{sparse}}^{(r)}$ is a sparse precision matrix. The $\boldsymbol{\Omega}_{\text{sparse}}^{(r)}$ is constructed through the following steps:

1. A dense Cholesky factor $\mathbf{L}^{(r)}$ is initially generated with $L_{ij}^{(r)} \stackrel{i.i.d.}{\sim} \mathcal{N}(0, 1)$ for $i > j$ and $L_{ii}^{(r)} \stackrel{i.i.d.}{\sim} \mathcal{N}(0, 0.1)$ for $i = 1, \dots, N$.
2. A binary mask $M_{\text{lower}}^{(r)}$ is generated as $M_{\text{lower}}^{(r)} \stackrel{i.i.d.}{\sim} \text{Binomial}(1, 1 - \kappa)$ for $i > j$, where κ controls the level of a sparsity.
3. A sparse Cholesky factor $\mathbf{L}_{\text{sparse}}^{(r)} = \mathbf{L}^{(r)} \circ M_{\text{lower}}^{(r)}$ is obtained, leading to $\boldsymbol{\Omega}_{\text{sparse}}^{(r)} = \mathbf{L}_{\text{sparse}}^{(r)} \mathbf{L}_{\text{sparse}}^{(r)\prime}$, where \circ is an element-wise multiplication.

We set $\kappa = 0.8$, thereby ensuring that 80% of the elements in $\boldsymbol{\Omega}_{\text{sparse}}^{(r)}$ are zero.

In the second simulation scheme, we employ a sparse MGARCH model with DCC configuration, adhering to the GARCH(1,1) specification delineated in Equation (3.1). The generation of $\mathbf{y}_t^{(r)}$ is formulated as

$$\mathbf{y}_t^{(r)} = \boldsymbol{\mu}_t^{(r)} + \left\{ \mathbf{D}_t^{(r)} \right\}^{1/2} \mathbf{L}_{\mathbf{S},t}^{-1} \boldsymbol{\varepsilon}_t^{(r)},$$

where $\mathbf{L}_{\mathbf{S},t}$ is a Cholesky factor of the sparse inverse correlation matrix

$$\mathbf{S}_t^{(r)} = \text{diag}\{\mathbf{P}_t^{(r)}\}^{-1/2} \mathbf{P}_t^{(r)} \text{diag}\{\mathbf{P}_t^{(r)}\}^{-1/2},$$

and $\mathbf{P}_t^{(r)}$ denotes a time-varying precision matrix. To generate $\mathbf{P}_t^{(r)}$ for each t , a random sparsity level κ_t is drawn from $\mathcal{U}(0.7, 0.9)$. A binomial-distributed, time-dependent sparsity mask is then formed, analogous to the first simulation design. Subsequently, for each t in the range $t = -50, -49, \dots, -1, 0, 1, \dots, 49, 50$, $\mathbf{P}_t^{(r)}$ is computed as

$$\mathbf{P}_t^{(r)} = \mathbf{L}_{\text{sparse},t}^{(r)} \mathbf{L}_{\text{sparse},t}^{(r)\prime} + \delta \boldsymbol{\Lambda}_t^{(r)},$$

where $\mathbf{L}_{\text{sparse},t}^{(r)}$ is generated in a manner consistent with the initial simulation setup, and $\boldsymbol{\Lambda}_t^{(r)}$ is drawn from a Wishart distribution with $T + 3$ degrees of freedom and identity matrix \mathbb{I}_N , denoted as $\boldsymbol{\Lambda}_t^{(r)} \stackrel{i.i.d.}{\sim} \mathcal{W}(T + 3, \mathbb{I}_N)$. The parameter δ is set to 0.1.

Incorporating $\boldsymbol{\Lambda}_t$ sampled from a Wishart distribution with $T + 3$ degrees of freedom and an identity scale matrix \mathbb{I}_N imposes specific structural properties on the simulation design. The Wishart distribution, a multivariate extension of the chi-squared distribution, is conventionally

employed for modeling the precision matrices of multivariate normal distributions. Opting for $T+3$ degrees of freedom engenders reduced variability around the scale matrix \mathbb{I}_N , thereby conferring greater stability—albeit with potential amplification—to the covariances in the precision matrix $\mathbf{P}_t^{(r)}$ due to the additive term $\delta\Lambda_t^{(r)}$.

The selection of \mathbb{I}_N as the scale matrix serves a normalization function, scaling the expected covariance structure to $(T+3)\mathbb{I}_N$. Consequently, it engenders a quasi-orthogonal structure in $\mathbf{P}_t^{(r)}$, rendering each variable nearly conditionally independent when Λ_t outweighs the sparse component $\mathbf{L}_{\text{sparse},t}^{(r)}\mathbf{L}_{\text{sparse},t}^{(r) \prime}$. The modulation parameter $\delta = 0.1$ subtly adjusts this quasi-orthogonality.

Additionally, the term $\delta\Lambda_t$ contributes a dense element to $\mathbf{P}_t^{(r)}$, transforming it into a heterogeneous matrix comprising both sparse and dense components. The magnitude of the dense component's influence on $\mathbf{P}_t^{(r)}$ is regulated by δ .

Remark 2. The construction of $\mathbf{P}_t^{(r)}$ requires further clarification, as it is not a purely sparse precision matrix; sparsity is imposed solely on its first term. The second term introduces density into the matrix, regulated by the parameter δ . This hybrid structure is motivated by extant literature that questions the empirical validity of sparsity assumptions, particularly in economics and finance. For instance, [Giannone, Lenza, and Primiceri \(2021\)](#) scrutinized multiple economic datasets and concluded that sparsity is generally not an inherent feature. Echoing this, they advocate for sparsity only when there is compelling a priori evidence supporting predictive models with a restricted set of explanatory variables ([Barigozzi and Brownlees \(2019\)](#)). Consequently, our simulation design incorporates both sparse and dense elements in $\mathbf{P}_t^{(r)}$ to more closely mimic the characteristics of real-world datasets. However, the incorporation of sparsity remains methodologically advantageous for computational tractability and interpretability. Additionally, sparse representations can offer a parsimonious yet effective approximation to complex, high-dimensional data structures, thus facilitating more manageable and insightful econometric analyses.

3.1 Simulation Results

In the simulation study, 100 replications are conducted for varying dimensions N and time periods T , specifically, $N = \{25, 50, 100, 125\}$ and $T = \{50, 100, 150, 200, 250\}$. Each estimation procedure involves 4,000 iterations, and a burn-in period of 2,000. In the implementation of the Gibbs sampling algorithm, the parameter c is set to 0.1, inducing a high level of sparsity in the model. For the Bayesian GARCH parameters, the mean values are uniformly set to zero: $\mu_{\omega_i} = \mu_{\theta_{0i}} = \mu_{\theta_{1i}} = \mu_a = \mu_b = \mu_{\gamma_i} = \mu_{\nu} = 0$. The variance parameters, excluding $\sigma_{\gamma_i}^2$, are uniformly assigned a value of 100: $\sigma_{\omega_i}^2 = \sigma_{\theta_{0i}}^2 = \sigma_{\theta_{1i}}^2 = \sigma_a^2 = \sigma_b^2 = \sigma_{\nu}^2 = 100$. The choice of $\sigma_{\gamma_i}^2 = 0.64^{-1}$ is made to achieve $\text{Var}(\gamma_i) \approx 0.57$ and $\text{Pr}(0 < \gamma_i < 1) \approx 0.58$, consistent with the findings in [Fioruci, Ehlers, and Andrade Filho \(2014\)](#). We find the Bayes estimate of the

inverse correlation matrix $\hat{\mathbf{S}}_t = \mathbb{E}(\mathbf{S}_t | \mathbf{Z})$. The performance of the proposed estimator for the inverse correlation matrix is evaluated using Root Mean Square Error (RMSE). Given that our methodology estimates time-varying inverse correlation matrices, the RMSE for each simulation design is computed as the temporal average of the estimated matrices. Specifically, the RMSE under the CCC and DCC cases are given by

$$\text{RMSE}_{\text{CCC}} = \left[\frac{2}{N(N-1)} \sum_{i=1}^N \sum_{j=1}^{i-1} \left(\frac{1}{T} \sum_{t=1}^T \hat{s}_{ij,t} - s_{ij}^o \right)^2 \right]^{1/2},$$

$$\text{RMSE}_{\text{DCC}} = \left[\frac{1}{T} \sum_{t=1}^T \frac{2}{N(N-1)} \sum_{i=1}^N \sum_{j=1}^{i-1} (\hat{s}_{ij,t} - s_{ij,t}^o)^2 \right]^{1/2},$$

where $\{\hat{s}_{ij,t}\}_{i,j=1,t=1}^{N,T} = \hat{\mathbf{S}}_t$ represents the elements of the estimated matrix, and $\{s_{ij,t}^o\}_{i,j=1,t=1}^{N,T} = \mathbf{S}_t^o$ denotes the elements of the known matrix.

For the purpose of comparative evaluation, the proposed estimator (NPC; Nonparanormal Partial Correlation) is compared with the method introduced by [Engle, Ledoit, and Wolf \(2019\)](#), which employs composite likelihood estimation in conjunction with nonlinear shrinkage (CNLS) for large-dimensional covariance matrix estimation within the DCC framework. Specifically, we utilized the DCC framework as proposed by [Aielli \(2013\)](#) for comparative analysis. However, the observed discrepancies between the models were minimal. To ensure a fair comparison and mitigate errors attributable to the inversion of large-dimensional correlation matrices, the RMSE between the estimated and true correlation matrices is calculated for this comparative method.

Table 1 presents the RMSEs of simulation outcomes for two methods: CNLS and NPC. Both methodologies exhibit suboptimal performance in scenarios characterized by CCC, chiefly due to their inherent proclivity for generating dense matrices. This is particularly discordant with the true Data Generating Process under the CCC framework, which is sparse and contains numerous zero elements. CNLS, not being predicated on a sparsity assumption, faces amplified issues when the underlying matrix is sparse, especially in small sample sizes. Contrary to intuition, enlarging the sample size fails to substantially enhance the performance of CNLS, which stems from the same absence of a sparsity assumption. In contrast, the NPC method, which also generates dense matrices, experiences less discrepancy due to its relative assumption on sparsity over the unconditional precision matrix. In the DCC setting, both methods demonstrate enhanced performance compared to the CCC scenario. As anticipated, the efficacy of both algorithms escalates with larger sample sizes. Notably, NPC exhibits superior performance in small sample scenarios, attributable to the Bayesian nature of the approach when priors are judiciously selected. Conversely, CNLS surpasses NPC in terms of performance when $N = 25$ and $N = 50$. For higher dimensions, it appears that a sample size exceeding 250 is requisite.

Table 1: RMSE for CCC and DCC Specifications

		CCC				DCC			
		Gaussian				Gaussian			
	T/N	25	50	100	125	25	50	100	125
NPC	50	0.1960	0.1616	0.1260	0.1141	0.1172	0.1064	0.0905	0.0854
	100	0.1957	0.1612	0.1250	0.1147	0.0936	0.0848	0.0759	0.0726
	150	0.1967	0.1602	0.1250	0.1140	0.0808	0.0739	0.0669	0.0646
	200	0.1947	0.1609	0.1257	0.1146	0.0721	0.0662	0.0606	0.0588
	250	0.1956	0.1592	0.1251	0.1140	0.0658	0.0606	0.0558	0.0546
	50	0.3640	0.4471	0.5728	0.5955	0.1332	0.1403	0.1546	0.1615
CNLS	100	0.3485	0.4538	0.5618	0.5921	0.0971	0.1001	0.1056	0.1083
	150	0.3479	0.4632	0.5450	0.6195	0.0804	0.0821	0.0850	0.0864
	200	0.3570	0.4531	0.5467	0.6017	0.0699	0.0711	0.0730	0.0741
	250	0.3682	0.4570	0.5593	0.6311	0.0623	0.0635	0.0649	0.0657
		t-distribution				t-distribution			
NPC	T/N	25	50	100	125	25	50	100	125
	50	0.1965	0.1611	0.1258	0.1146	0.1256	0.1121	0.0908	0.0859
	100	0.1913	0.1613	0.1243	0.1142	0.0949	0.0895	0.0773	0.0735
	150	0.1932	0.1601	0.1249	0.1154	0.0819	0.0802	0.0698	0.0665
	200	0.1954	0.1615	0.1251	0.1148	0.0730	0.0719	0.0657	0.0616
	250	0.1938	0.1600	0.1247	0.1144	0.0672	0.0656	0.0610	0.0566
CNLS	50	0.3410	0.4744	0.5711	0.5603	0.1334	0.1410	0.1549	0.1618
	100	0.3539	0.4503	0.5805	0.5939	0.0976	0.1009	0.1056	0.1094
	150	0.3683	0.4571	0.5737	0.6127	0.0801	0.0821	0.0854	0.0868
	200	0.3417	0.4469	0.5705	0.6071	0.0698	0.0710	0.0736	0.0742
	250	0.3569	0.4609	0.5771	0.6003	0.0631	0.0635	0.0652	0.0659

Notes: In the simulation study, each estimation procedure involved 100 replications, 4,000 iterations, and a burn-in period of 2,000. The Root Mean Square Error (RMSE) was computed for both the Constant Conditional Correlation (CCC) and Dynamic Conditional Correlation (DCC) cases. Specifically, the RMSE for the CCC case is given by $\text{RMSE}_{\text{CCC}} = [\frac{2}{N(N-1)} \sum_{i=1}^N \sum_{j=1}^{i-1} (\frac{1}{T} \sum_{t=1}^T \hat{s}_{ij,t} - s_{ij}^o)^2]^{1/2}$ and for the DCC case, it is defined as $\text{RMSE}_{\text{DCC}} = [\frac{1}{T} \sum_{t=1}^T \frac{2}{N(N-1)} \sum_{i=1}^N \sum_{j=1}^{i-1} (\hat{s}_{ij,t} - s_{ij,t}^o)^2]^{1/2}$.

Regarding the distributional assumptions, negligible differences were observed between Gaussian and t -distributions due to the fact that both distributions contribute only indirectly to the construction of standardized residuals.

4 Empirical Applications

Understanding the nuanced relationships between economic indicators is paramount in studying financial markets. Our exploration of foreign stock price indexes, stock prices, and exchange rates underscores global and localized influences. Conditional correlations illuminate these relationships but might blur the lines between broad global events and specific bilateral interactions. To sharpen our analysis, we introduce dynamic conditional partial correlations. Through three empirical applications—conditional dependencies among international stock price indices, stock prices of firms in the S&P 100, and foreign exchange rate volatility—we equip both conditional and partial correlations alongside their unconditional structures, achieving a more encompassing grasp of the financial landscape.

In each application, we examine both the unconditional dependence structures and the posterior mean of dynamic partial correlations. The former is derived from partial correlation matrices predicated on Ω as defined in Equation (2.4), while the latter originates from the standard conjugate Wishart prior. The posterior of the unconditional partial correlations, λ_{ij} , is determined as per Equation (2.6):

$$\lambda_{ij} = \begin{cases} -\omega_{ij}/\sqrt{\omega_{ii}\omega_{jj}}, & \text{for } i \neq j \\ 1 & \text{for } i = j \end{cases},$$

where $\omega_{ij} = \{\Omega\}_{i,j=1}^N$ for $i, j = 1, \dots, N$. The posterior mean is subsequently calculated from MCMC draws of these distributions.

For the unconditional posterior partial correlations based on the standard conjugate Wishart prior, we specify a prior for the precision matrix $\tilde{\Omega} \sim \mathcal{W}(3, \mathbb{I})$, where \mathbb{I} represents the identity matrix. By virtue of conjugacy, the posterior distribution is $\tilde{\Omega}|\mathbf{Z} \sim \mathcal{W}(T+3, (\mathbb{I} + \Sigma)^{-1})$, where $\Sigma = \mathbf{Z}'\mathbf{Z}$. The posterior partial correlation $\tilde{\lambda}_{ij}$ is then defined as:

$$\tilde{\lambda}_{ij} = \begin{cases} -\tilde{\omega}_{ij}/\sqrt{\tilde{\omega}_{ii}\tilde{\omega}_{jj}}, & \text{for } i \neq j \\ 1 & \text{for } i = j \end{cases},$$

with $\tilde{\omega}_{ij} = \{\tilde{\Omega}\}_{i,j=1}^N$ for $i, j = 1, \dots, N$. The posterior mean is computed analogously to the non-conjugate case.

Edges in the dependence structure matrix are assigned based on a comparison between

λ_{ij} and $\tilde{\lambda}_{ij}$. Specifically, an edge is posited if $\lambda_{ij}/\tilde{\lambda}_{ij} > 0.5$; otherwise, it is omitted. This methodology aligns with [Mulgrave and Ghosal \(2022\)](#), albeit with a modification: we employ the standard Wishart prior for the unconditional precision matrix rather than directly for the inverse correlation matrix, as is the case in [Mulgrave and Ghosal \(2023\)](#).

For model estimation, 4,000 iterations with a 2,000 burn-in period are implemented. Volatility is quantified as $\text{Volatility} = 100 \log \left(\frac{p_t}{p_{t-1}} \right)$, where p_t denotes the closing price of the respective stock index. In accordance with the simulation analyses, we present the corrected DCC (cDCC) estimates [Engle, Ledoit, and Wolf \(2019\)](#) for comparative purposes.

4.1 Foreign Stock Price Indexes

Foreign Stock Price Indexes are heavily influenced by global factors, often overshadowing country-specific events and leading to closely moving correlations. These correlations can be traced back to international monetary policies, geopolitical tensions, and broad economic events. Given our interconnected financial markets, disturbances in one significant market typically resonate across others. While partial correlations aim to highlight bilateral relationships by filtering out some prominent global influences, they may not entirely remove unobservable common factors, leaving room for further exploration in the peaks and troughs of conditional correlations.

Utilizing a harmonized time series from a selected dataset of stock price indices—Dow Jones and NASDAQ in the US, DAX in Germany, CAC40 in France, and NIKKEI in Japan—the study spans 7,600 trading days from January 4, 1991, to August 31, 2023, sourced from Google Finance. This common sample size is chosen to mitigate the discrepancies in trading days across the five indices, attributed to factors such as national holidays, time zones, and market-specific practices, thereby facilitating consistent cross-market comparisons and analyses. The unconditional dependence structure of the foreign stock indexes presents fully connected graphs. Consequently, we exclude the figure due to its limited informational value.

Figure 1 presents a detailed examination of the cDCC and the dynamic conditional partial correlations between major stock indices: Dow Jones and NASDAQ in the US, DAX in Germany, CAC40 in France, and NIKKEI in Japan from 1991 to 2023. The cDCCs between these two US indices, as expected, show a consistently high correlation over time, reflecting the closely tied nature of their underlying economies. Notable spikes in correlation can be observed during significant economic downturns, such as the dot-com bubble burst around 2000 and the global financial crisis in 2008. However, the dynamic conditional partial correlations present a more muted response to these events, suggesting that once the broader influences are factored out, the intrinsic interdependence between Dow Jones & NASDAQ remains relatively stable. The correlations between the US and German indices fluctuate considerably over the years. The pronounced co-movements, especially during periods of global turbulence, under-

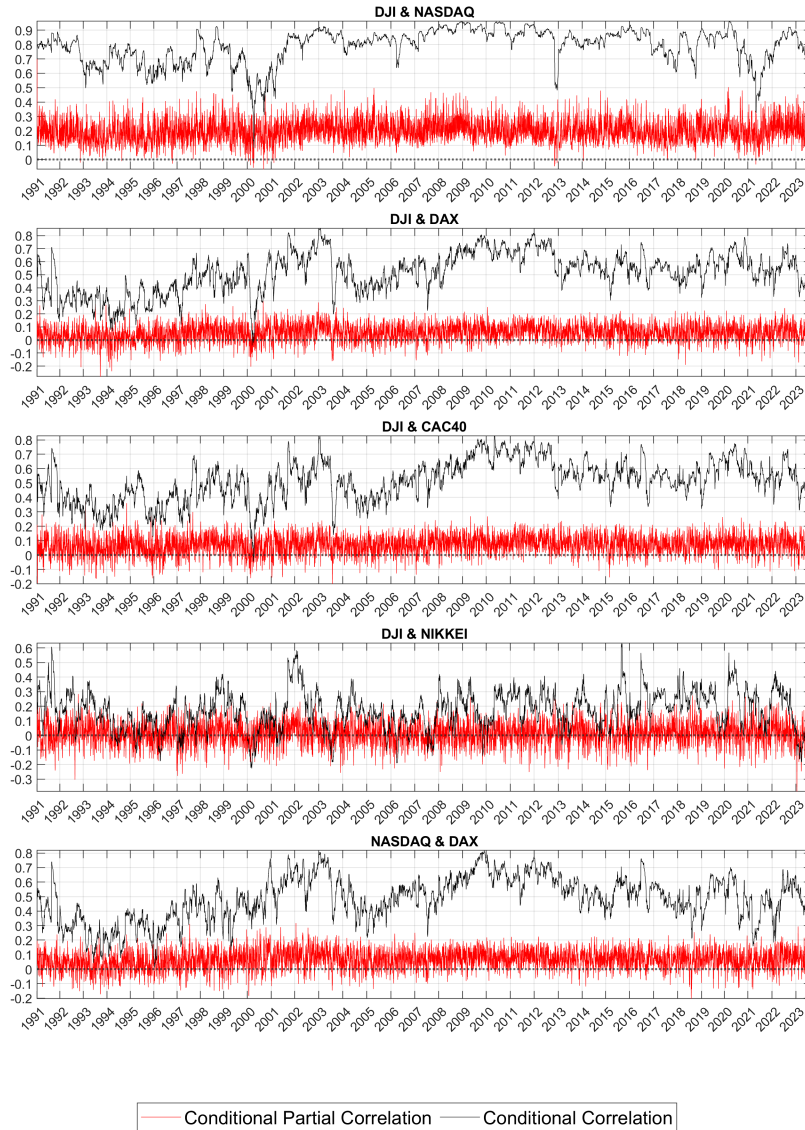


Figure 1: Dynamic Conditional (Partial) Correlations: Foreign Stock Indexes 1

Notes: The dataset has been sourced from Google Finance, spanning the period from January 4, 1991, to August 31, 2023. The measure for volatility is calculated using the formula: Volatility = $100 \log(p_t/p_{t-1})$, where p_t represents the closing price of the respective stock index. The abbreviations for the stock indexes are as follows: DJI denotes the Dow Jones Industrial Average, NASDAQ signifies the National Association of Securities Dealers Automated Quotations, DAX stands for Deutscher Aktienindex, CAC40 is an acronym for Cotation AssistÃ©e en Continu 40, and NIKKEI represents the Nikkei 225 Stock Average.

score the synchronization of global markets. The early 2020s again stand out due to the global pandemic's effects. However, the partial correlations tell a more subdued story, implying that their direct interplay is not as volatile as simple correlations might suggest once other variables are controlled for. Much like the DAX, the French CAC40 index also exhibits increased synchronicity with the Dow Jones during global economic downturns. The dynamic conditional partial correlations, though lower in magnitude, display similar patterns of divergence, especially during crisis periods. The Japanese market, represented by the NIKKEI, demonstrates unique dynamics. While the DCCs show increased alignment during universal market stressors, there are periods where the NIKKEI seems to march to its own beat. The conditional partial correlations here offer some fascinating insights, indicating a more consistent and tempered relationship when other market influences are parsed out. The final graph delves into the interactions between the tech-heavy NASDAQ and Germany's DAX. Both being bellwethers of their respective economies, they show pronounced DCCs during global market upheavals. However, the partial correlations, while still reactive, maintain a more measured trajectory.

Figure 2 displays the dynamics of conditional correlations and partial correlations for the rest of the stock indices. In NASDAQ and CAC40, the partial correlations exhibit nuanced responses through pivotal events. For instance, during the tech bubble around 2000, while conditional correlations surged, partial correlations indicated a slightly different response, perhaps due to underlying market structures and policies differentiating the two. Moving to the 2008 financial crisis, conditional correlations displayed a synchronized reaction, yet the partial correlations illustrated that when the broader market influences were removed, the NASDAQ and CAC40 did not move in perfect tandem. After 2010, during events such as the Eurozone crisis and Brexit uncertainties, the partial correlations oscillated more frequently, signifying underlying factors driving these markets apart. In NASDAQ and NIKKEI, the late 1990s saw both metrics reacting to the Asian financial crisis. Post-2010, while the conditional correlations remained largely consistent, the partial correlations showcased an interesting divergence around the mid-2010s, emphasizing a decoupling possibly due to Japan's unique monetary policy decisions versus NASDAQ's tech sector growth. In DAX and CAC40, the ascent towards the 2008 financial crisis witnessed a heightened co-movement in conditional correlations. However, the partial correlations during this period and post-2010 painted a diverse picture. Specifically, during the Greek debt crisis, the partial correlations between DAX and CAC40 displayed starker fluctuations than their conditional counterparts, suggesting inherent market differences in the two economies' reactions to shared European events. In DAX & NIKKEI, the conditional and partial correlations displayed significant fluctuations around events like the early 2000s recession. However, post-2010, while conditional correlations suggested a heightened synchronization, the partial correlations hinted at unique market dynamics, possibly arising from Germany's economic decisions concerning Japan's deflationary challenges and resulting policies.

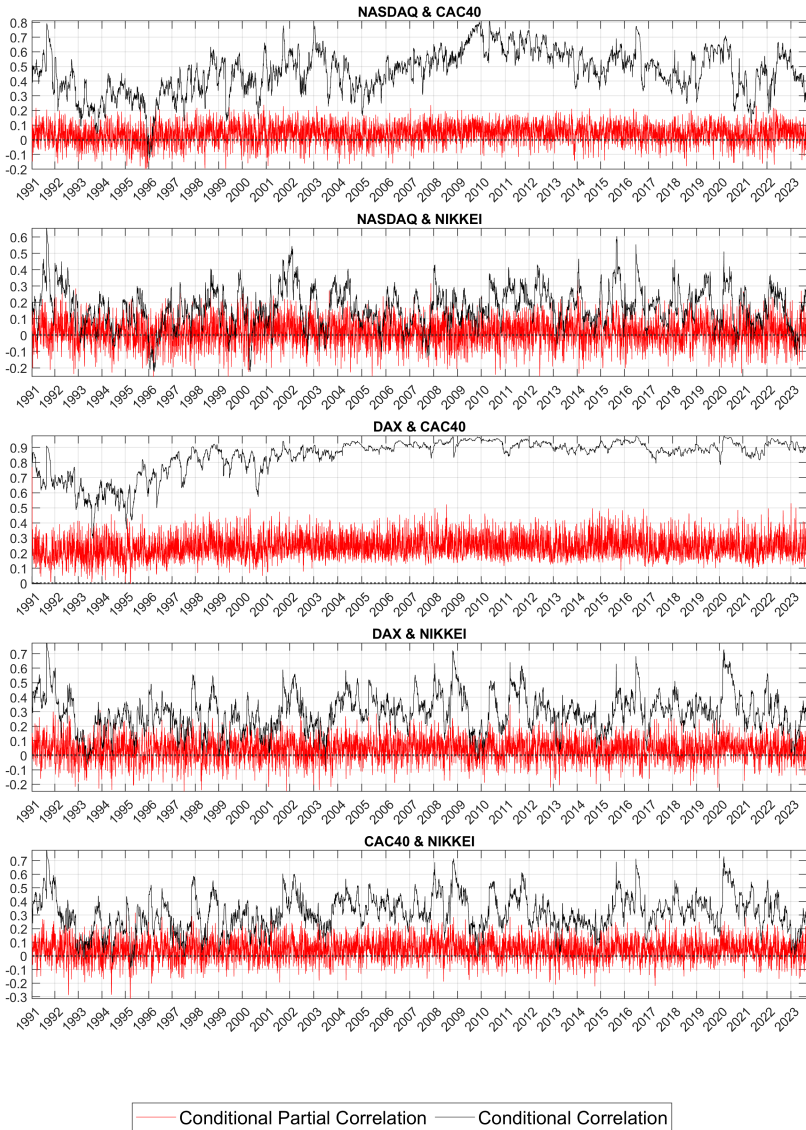


Figure 2: Dynamic Conditional (Partial) Correlations: Foreign Stock Indexes 2

Notes: The dataset has been sourced from Google Finance, spanning the period from January 4, 1991, to August 31, 2023. The measure for volatility is calculated using the formula: Volatility = $100 \log(p_t/p_{t-1})$, where p_t represents the closing price of the respective stock index. The abbreviations for the stock indexes are as follows: DJI denotes the Dow Jones Industrial Average, NASDAQ signifies the National Association of Securities Dealers Automated Quotations, DAX stands for Deutscher Aktienindex, CAC40 is an acronym for Cotation AssistÃ©e en Continu 40, and NIKKEI represents the Nikkei 225 Stock Average.

In CAC40 and NIKKEI, the shared market responses of the early 2000s, likely influenced by global events, manifested in both types of correlations. However, post-2010, while conditional correlations portrayed a relatively synchronized dance, partial correlations highlighted distinct ebbs and flows. Specifically, around 2019, as global markets wrestled with trade tensions and slowing growth, the partial correlations between CAC40 and NIKKEI experienced increased volatility, highlighting a divergence in their underlying market dynamics, potentially reflecting their respective domestic policies and economic strategies.

Regarding the global common factors, during the period corresponding to the COVID-19 pandemic, Figures 1 and 2 depict marked fluctuations in both conditional correlations and conditional partial correlations across the various market pairs. The conditional correlations indicate pronounced synchronous movements between markets, suggesting a global response to pervasive external shocks, likely anchored by the pandemic's wide-ranging effects. In contrast, by controlling for other market influences, the conditional partial correlations unveil nuanced inter-market dynamics, revealing differential responses of individual markets to the global shock. This variance in the conditional partial correlations underscores each country's unique economic landscapes and policy interventions during this period, emphasizing the pandemic's differentiated impact across global financial markets.

4.2 Stock Prices: S&P 100

The behavior exhibited by Individual Stock Prices is markedly different, predominantly shaped by company-centric determinants, be it earnings reports, decisions by management, or industry-specific news. Such idiosyncratic movements make their volatilities more distinct, predominantly bearing the imprints of activities intrinsic to the firm. The disparity between correlations and partial correlations in this sphere is noticeably accentuated, underscoring the diminished impact of ubiquitous global factors on standalone stock trajectories. However, even in this context, one must recognize the possible residual influence of unobservable global elements when analyzing partial correlations.

We encompass a panel of 98 firms diversified across multiple industry sectors, delineated in Table A1 of the Appendix. The temporal scope extends from September 2, 2016, to August 31, 2023, amounting to 1,760 trading days, sourced from Google and Yahoo Finance. Predominantly, these firms constitute the S&P 100 index during the sample period. Utilizing closing stock prices, we derive hundredfold log-returns on a daily basis.

Figure 3 illustrates the unconditional structure dependence structure for a panel of 98 firms spanning various industry sectors over the period from September 2, 2016, to August 31, 2023. The firms, mainly constituents of the S&P 100 index during the sample period, have their relationships mapped based on financial data sourced from Google and Yahoo Finance. Each node in the graph represents an individual stock ticker, and the degree of each node conveys the

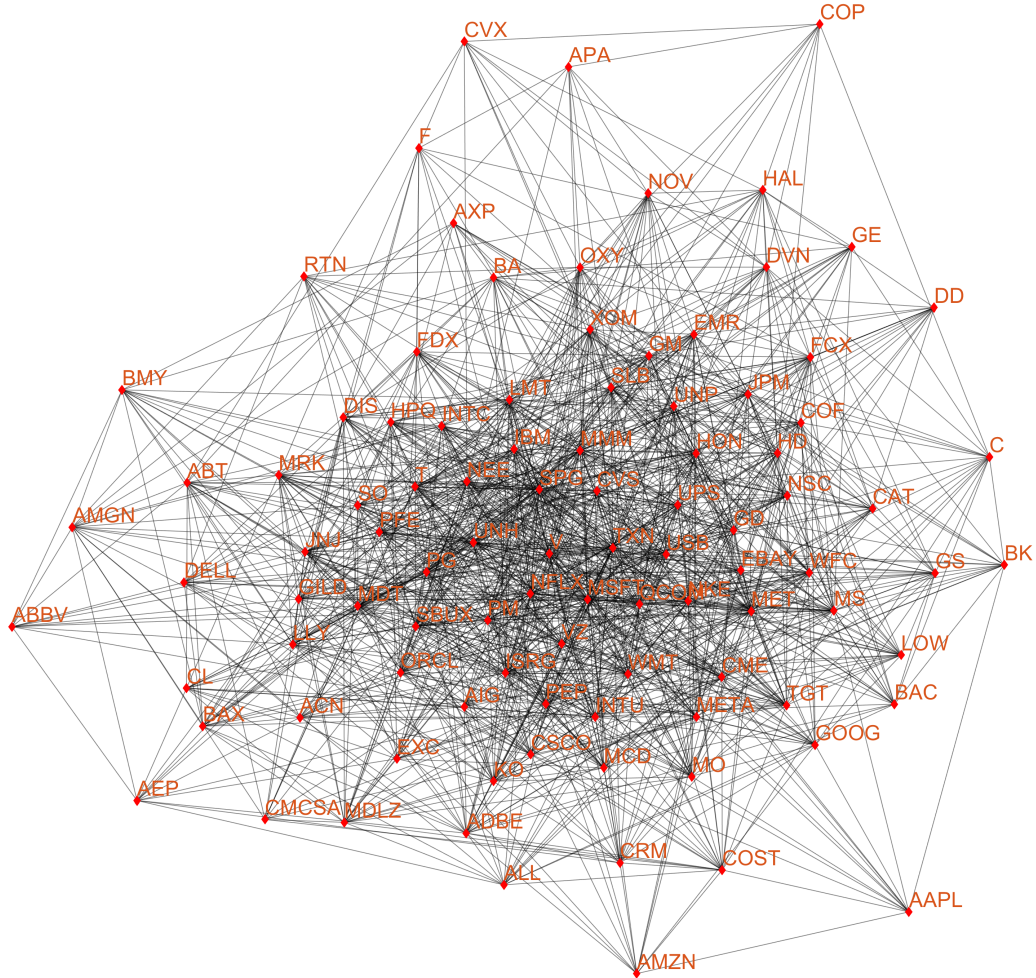


Figure 3: Unconditional Dependence Structure: Sep. 2016 – Aug. 2023

Notes: The degree of each node, corresponding to individual stock tickers, is enumerated as follows: AAPL(13), ABBV(12), ABT(23), ACN(19), ADBE(26), AEP(13), AIG(20), ALL(18), AMZN(14), APA(10), AXP(13), BA(22), BAC(19), BAX(20), BK(16), BMY(17), C(18), CAT(20), CL(16), CMCSA(13), CME(26), COF(25), COP(10), COST(23), CRM(21), CSCCO(25), CVS(31), CVX(11), DD(16), DELL(16), DIS(26), DVN(22), EBAY(22), EMR(30), EXC(20), F(11), FCX(27), FDX(24), GD(29), GE(16), GILD(32), GM(32), GOOG(23), GS(23), HAL(21), HD(29), HON(39), HPQ(31), IBM(31), INTC(32), INTU(39), ISRG(43), JNJ(31), JPM(32), K(29), LLY(29), LMT(40), LOW(22), MCD(27), MDLZ(24), MDT(38), MET(43), META(29), MMM(46), MO(26), MRK(30), MS(37), MSFT(51), NEE(41), NFLX(42), NKE(37), NOV(20), NSC(28), ORCL(31), OXY(26), PEP(38), PFE(33), PG(38), PM(29), QCOM(42), RTN(15), SBUX(34), SLB(35), SO(28), SPG(52), T(31), TGT(31), TXN(42), UNH(42), UPN(31), UPS(31), USB(37), V(48), VZ(33), WFC(33), WMT(38), XOM(35). The degree of each ticker is encapsulated within parentheses. For an exhaustive account of each ticker, see Appendix C.

number of direct connections it has within the network. Given the total possible connections of 4,753 ($= \binom{98}{2}$), and the 1,348 observed connections (summing up the degrees and dividing by 2), the graph's density is approximately 0.284, suggesting a moderately sparse network of connections. In the derived structure, a stock with the maximum degree is selected to represent each Global Industry Classification Standard (GICS) sector for clarity in depiction. Specifically, representatives include FCX for Materials, ISRG for Health Care, MMM for Industrials, MSFT for Information Technology, NEE for Utilities, NFLX for Communication Services, NKE for Consumer Discretionary, SPG for Financials, WMT for Consumer Staples, and XOM for Energy. Subsequent figures present the pairwise conditional correlations and conditional partial correlations for the selected stocks, corresponding to the edges delineated in Figure 3. To enhance visual representation, the dynamic conditional partial correlations have been scaled by a factor of 10.

Figure 4 represents the conditional and partial correlations for selected stock pairs from September 2, 2016, to August 31, 2023. The conditional correlation between FCX and MMM follows a stable trajectory compared to the conditional partial correlation. This stability in conditional correlation reflects the direct relationship between the stocks, independent of other factors. The more dynamic nature of the partial correlations suggests that the relationship exhibits volatility when external influences are accounted for. Fluctuations between 2018 and 2019 may be linked to trade tensions and tariff policies, with both the materials and industrial sectors directly impacted. A noticeable dip around 2020 in the conditional correlations can underscore the pandemic's influence on these sectors. Both FCX and MSFT experience a rise in conditional and partial correlations leading up to 2021, possibly reflecting the recovery of the materials sector and the surge in tech companies like MSFT, driven by a widespread pivot to digital platforms. This rise is followed by a decline post-2021 in the partial correlation, hinting at market stabilization and the waning immediate effects of the pandemic.

The conditional correlation between ISRG and NEE remains largely consistent throughout the period, with a distinct rise around 2020. This rise coincides with the pandemic, emphasizing the significance of healthcare organizations like ISRG and the consistent demand for utilities like NEE. The more pronounced ascent in the conditional partial correlations during 2020 suggests a unique interrelation in their performances, possibly due to specific external events stemming from the pandemic. The conditional correlation between MMM and MSFT shows a marked dip between 2019 and 2020, highlighting the pandemic's divergent impacts: while MMM contended with disruptions, MSFT thrived due to the digital shift. The conditional partial correlation reveals a similar pattern, albeit with increased volatility, indicating heightened sensitivity to market events once other influences are isolated. The subsequent recovery post-2020 in the partial correlations signals a stabilization in sectors and a sustained tech surge.

In 2018, MSFT and ISRG exhibited a drop in conditional correlation, possibly reflecting

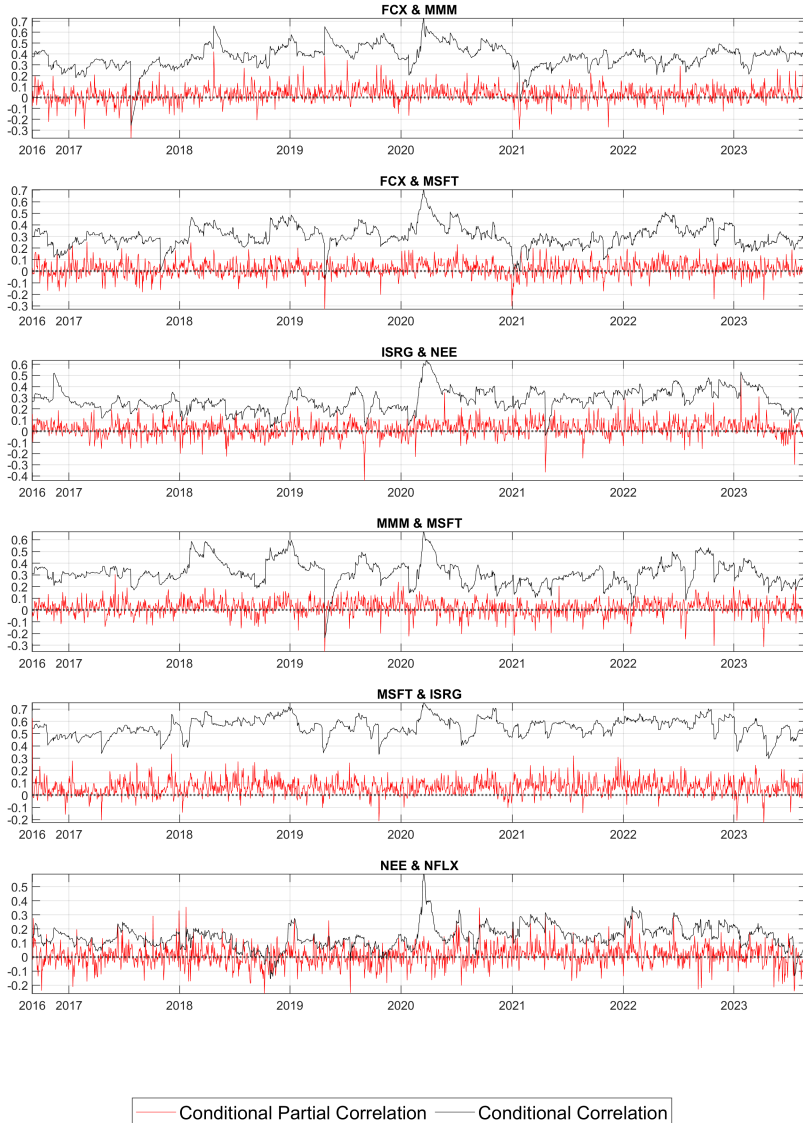


Figure 4: Dynamic Conditional (Partial) Correlations: Stock Volatilities 1

Notes: The figure describes the dynamic conditional correlations and dynamic conditional partial correlations among stock price volatilities for sectors characterized by a high degree of unconditional dependence. Stock ticker symbols corresponding to each sector are delineated as follows: Materials (FCX), Health Care (ISRG), Industrials (MMM), Information Technology (MSFT), Utilities (NEE), Communication Services (NFLX), Consumer Discretionary (NKE), Financials (SPG), Consumer Staples (WMT), and Energy (XOM). A comprehensive list of associated stock tickers can be found in Appendix C. To enhance visual representation, the dynamic conditional partial correlations have been scaled by a factor of 10.

market trends at the time, including rising interest rates and looming economic slowdowns. Regulatory uncertainties might have affected healthcare companies like ISRG, and data privacy concerns likely posed challenges for tech giants like MSFT. The pronounced variability in both conditional and partial correlations between 2019 and 2020 corresponds with the pandemic's onset. The technology sector, represented by MSFT, adapted to the shift to remote work and increased reliance on digital platforms, while healthcare entities like ISRG navigated the extensive implications of the pandemic. Lastly, NEE and NFLX maintain a stable conditional correlation, mirroring their partial correlations. Their consistent interrelation for most of the period may be interrupted by a significant increase in both metrics in 2020, pointing to the surge in demand for home entertainment via platforms like NFLX during lockdowns and the simultaneous rise in the essential nature of utilities, as evidenced by NEE.

NEE in Utilities and XOM in Energy demonstrate variable partial correlations throughout the period, with noticeable divergences around 2019 and 2020. The energy sector's challenges during these years, stemming from volatile oil prices and a transition to sustainable energy, likely contributed to the increased conditional partial correlation with NEE. Such trends underscore the changing interrelations as both sectors navigated global energy transitions and mounting environmental pressures. The conditional partial correlation between NFLX in Communication Services and NKE in Consumer Discretionary maintains stability but showcases peaks, particularly around 2020. The pandemic-induced rise in 2020 highlights the synergistic bond between entertainment and consumer products. Lockdown measures fueled a surge in home entertainment while companies like NKE pivoted towards direct-to-consumer and digital strategies, resulting in simultaneous sectoral growth. NKE and SPG in Real Estate depict active interactions, primarily from 2018 to 2021. Given SPG's retail real estate emphasis, its trajectory closely aligns with retail brands such as NKE. The oscillations likely reflect the shifting retail environment during this time, with physical stores contending against e-commerce and the pandemic's push for online retail in 2020, impacting both companies.

The interrelation between NKE and WMT in Consumer Staples undergoes pronounced changes, particularly post-2020. As WMT enhanced its online reach and diversified its product range, including athletic wear, the contemporaneous expansion approaches of both firms, especially in e-commerce, can elucidate the increased partial correlations after 2020. SPG and WMT exhibit fluctuating conditional partial correlations throughout the period. The rising trend around 2019-2020 corresponds with the retail sector's challenges. As the pandemic amplified e-commerce's role, traditional retail spaces, represented by SPG, had to evolve. Concurrently, WMT fortified its digital and omnichannel approaches, deepening their mutual influences. The conditional partial correlation between WMT and XOM remains largely consistent, albeit with discernible variations around 2018 and 2020. Given the global economic sensitivities of both firms, shared reactions to events like oil price fluctuations, 2018's trade tensions, and 2020's

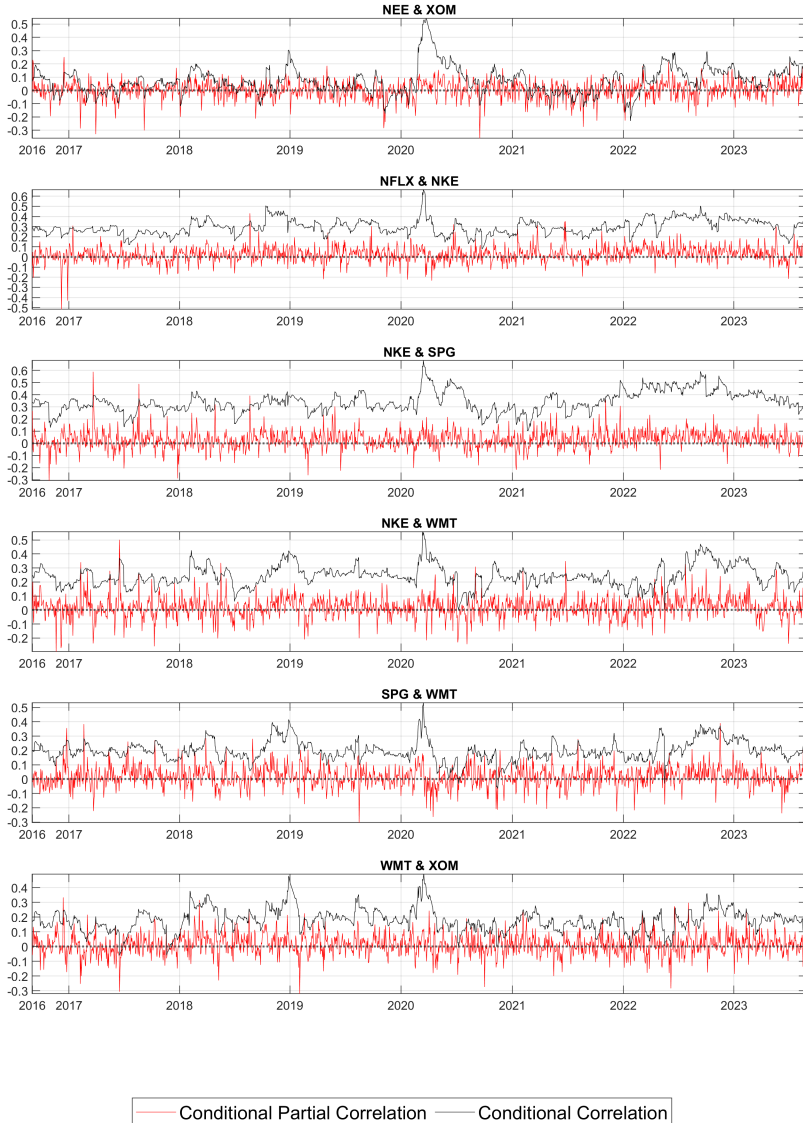


Figure 5: Dynamic Conditional (Partial) Correlations: Stock Volatilities 2

Notes: The figure describes the dynamic conditional correlations and dynamic conditional partial correlations among stock price volatilities for sectors characterized by a high degree of unconditional dependence. Stock ticker symbols corresponding to each sector are delineated as follows: Materials (FCX), Health Care (ISRG), Industrials (MMM), Information Technology (MSFT), Utilities (NEE), Communication Services (NFLX), Consumer Discretionary (NKE), Financials (SPG), Consumer Staples (WMT), and Energy (XOM). A comprehensive list of associated stock tickers can be found in Appendix C. To enhance visual representation, the dynamic conditional partial correlations have been scaled by a factor of 10.

pandemic challenges are evident in the recorded patterns.

Reexamine Figures 4 and 5, the partial correlations appear to underscore downturns in conditional correlations, potentially pointing to stocks' enhanced responsiveness to unfavorable events when general market factors are isolated. Such patterns might be driven by mechanisms like "stop-loss orders" or widespread "flight to quality" reactions during market declines. Concurrent rises and falls in both indicators suggest inherent ties between stocks, potentially hinting at shared external stimuli and congruent market perceptions. This alignment could capture intrinsic business interconnections, region-centric events influencing both stocks or dominant market narratives shaping investor perspectives.

4.3 Exchange Rates

Exchange Rates navigate through a multifarious environment, sculpted by various influences ranging from state-driven monetary and fiscal directives to expansive global economic paradigms. Though susceptible to exogenous shocks, such as geopolitical events, the crux of their dynamics often resides in the bilateral economic and trade ties. The evident distinction between standard and partial correlations in this realm offers insights into the myriad determinants steering exchange rate fluctuations. Nevertheless, when dissecting these correlations, remaining cognizant of the potential residuals from unobservable global determinants is pivotal.

Using daily foreign exchange rate data from January 4, 1999, to January 4, 2019, we compiled a total of observations, sourced from WRDS(Wharton Research Data Services). This period post-dates the introduction of the Euro on January 1, 1999. The data includes the exchange rates of 23 countries and the Eurozone. These countries are Australia, Brazil, Canada, China, Denmark, Hong Kong, India, Japan, Korea, Malaysia, Mexico, New Zealand, Norway, Singapore, South Africa, Sri Lanka, Sweden, Switzerland, Taiwan, Thailand, the United Kingdom, Venezuela, and the Eurozone.

Figure 6 describes an unconditional structure dependence derived from daily foreign exchange rate data between January 4, 1999, and January 4, 2019, revealing the intricate interconnections among the exchange rates of 23 countries and the Eurozone. Each node in the figure, delineated by country or region, illustrates the currency's degree of connectivity with other entities, signifying its interconnectedness within the examined foreign exchange network. Notably, Singapore, with a degree of 21, emerges as the most interconnected, implying a heightened level of interdependency with other currencies, while Denmark, with a degree of 5, exhibits the least. For analytical precision, we employ Singapore as a benchmark case, given its preeminent connectivity in terms of foreign exchange rate volatility. Further, we selectively focus on nations with significant economic stature, including China, Japan, the UK, and the Eurozone.

Figure 7 delineates the conditional and partial correlations of foreign exchange volatility between Singapore with both China and Japan. The intricate dynamics visible upon close in-

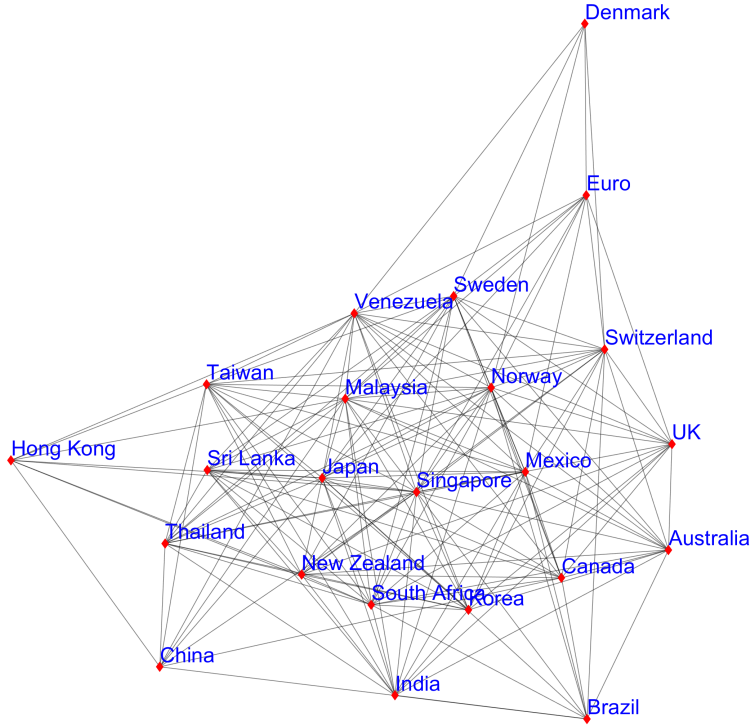


Figure 6: Unconditional Dependence Structure (1999–2019)

Notes: The degree of each node, corresponding to individual stock tickers, is enumerated as follows: Australia(14), Brazil(10), Canada(14), China(9), Denmark(5), Hong Kong(8), India(14), Japan(19), Korea(14), Malaysia(18), Mexico(17), New Zealand(15), Norway(19), Singapore(21), South Africa(17), Sri Lanka(13), Sweden(17), Switzerland(16), Taiwan(15), Thailand(14), United Kingdom(13), Venezuela(18), Eurozone(10). The degree of each ticker is encapsulated within parentheses.

spection shed light on the profound interplay of international and nation-specific events affecting these correlations. In the case of Singapore and China, the partial correlation exhibits distinct fluctuations over the illustrated period. A peak between 2012 and 2013 is especially noteworthy, eclipsing even the rise around 2008. This period, marking a deceleration in China's brisk economic growth, brought to the fore apprehensions regarding China's export-oriented economic model and the longevity of its stellar growth trajectories. To address these concerns, the Chinese authorities embarked on reforms, steering the economy towards a consumption-driven paradigm. Simultaneously, reservations about China's informal banking sector and escalating regional government debts emerged. Given Singapore's stature as a pivotal financial nexus and its deep-rooted trade connections with China, such developments likely magnified the impact on Singapore's currency volatility in relation to the Chinese economic shifts. The surge in partial

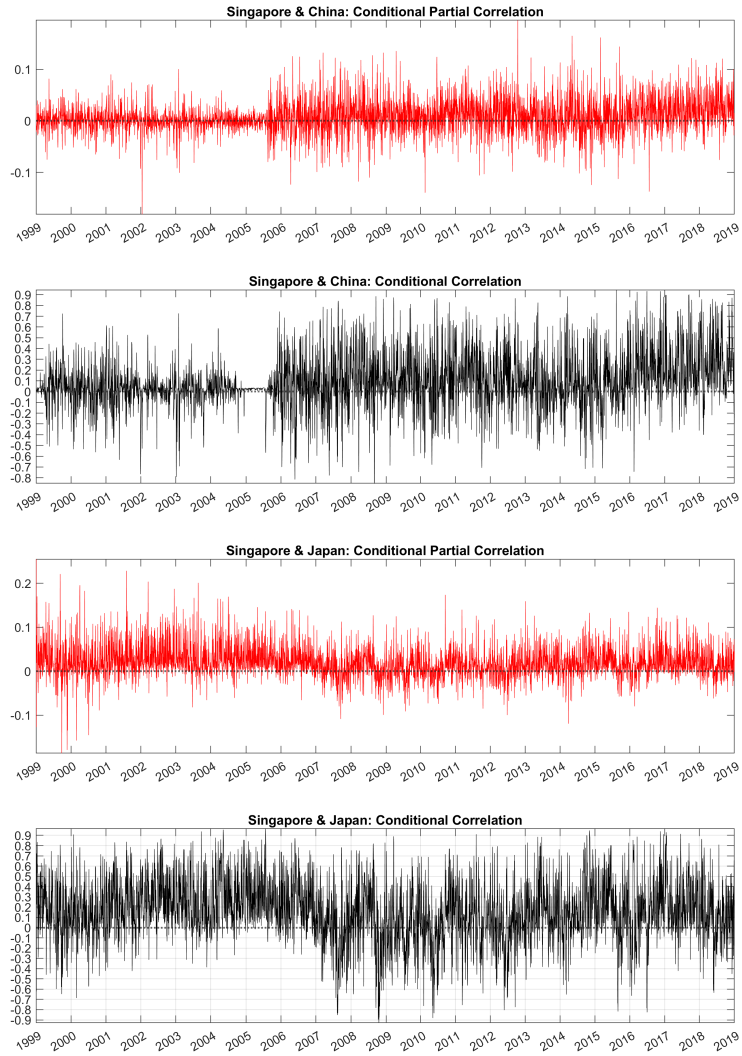


Figure 7: Dynamic Conditional (Partial) Correlations: Foreign Exchange Rates 1

Notes: The data encompasses a time span from January 4, 1999, to January 4, 2019. Volatility of the foreign exchange rate is quantified using the formula $\text{Volatility} = 100 \log \left(\frac{x_t}{x_{t-1}} \right)$, where x_t denotes the foreign exchange rate for the country under consideration at time t .

correlation arguably represents this enhanced interrelation. On the other hand, the conditional correlation, reflecting the synchronized movement of foreign exchange volatilities between the two nations devoid of external variable interference, retains a semblance of stability over the two decades. Nonetheless, it does showcase discernible oscillations. The perturbations around 2008 resonate with the global financial turmoil, mirroring the augmented volatility and ambivalence rampant in global financial arenas at that juncture.

In the analysis of Singapore and Japan, the displayed two-decade trajectory exhibits pronounced oscillations, epitomizing the multifaceted influences at play. The bedrock of Singapore and Japan's economic rapport has historically been their solid bilateral trade engagement. Perturbations in this equilibrium, spurred by the footprint of Japanese multinational entities in Singapore and evolving trade magnitudes, might have instigated currency rate perturbations. Monetary policy dichotomies further augmented this landscape. Japan's unconventional monetary stances, encompassing its foray into negative interest terrains and quantitative easing to address entrenched deflation, stood in stark juxtaposition to Singapore's strategy of optimizing its currency rate for competitive edge and inflation regulation. Such incongruence potentially infused the market with turbulence as it grappled with shifts in interest benchmarks and liquidity scenarios.

Moreover, Singapore and Japan were vulnerable to the ebb and flow of regional geopolitical events, trade dynamics, and shifts in regional power balances. Notable events, such as the South China Sea discord or North Korean ballistic endeavors, could have had bearings on their currency valuations. Initiatives from Japan, exemplified by Abenomics, elicited anticipative currency adjustments, which echoed in Singapore's foreign exchange milieu owing to its central position in the financial sphere. In conclusion, episodic exchange rate volatilities might also be attributed to tourism fluxes, swayed by events like the SARS epidemic in the early 2000s or the 2011 Fukushima catastrophe.

Figure 8 underscores the dynamics of conditional and partial correlations of foreign exchange volatility involving Singapore paired with the UK and the Euro. Observing the conditional partial correlation between Singapore and the UK, the correlations have discernible stability, with sporadic peaks and troughs. Some of the evident peaks are around 2008 and between 2015 and 2016. The 2008 peak can be attributed to the global financial crisis, which undoubtedly influenced foreign exchange markets globally. The subsequent peak around 2015-2016 aligns with the period leading up to the Brexit referendum. The uncertainty surrounding the UK's decision to leave the Euro likely directly impacted its currency, an effect that resonated in its correlation with the Singaporean dollar, given the economic ties between the two nations. Similarly, the partial correlation plot accentuates specific periods of heightened volatility for Singapore and the Euro. The 2008 global financial crisis is once again visible as a defining moment. Furthermore, the extended heightened volatility between 2010 and 2012 correlates

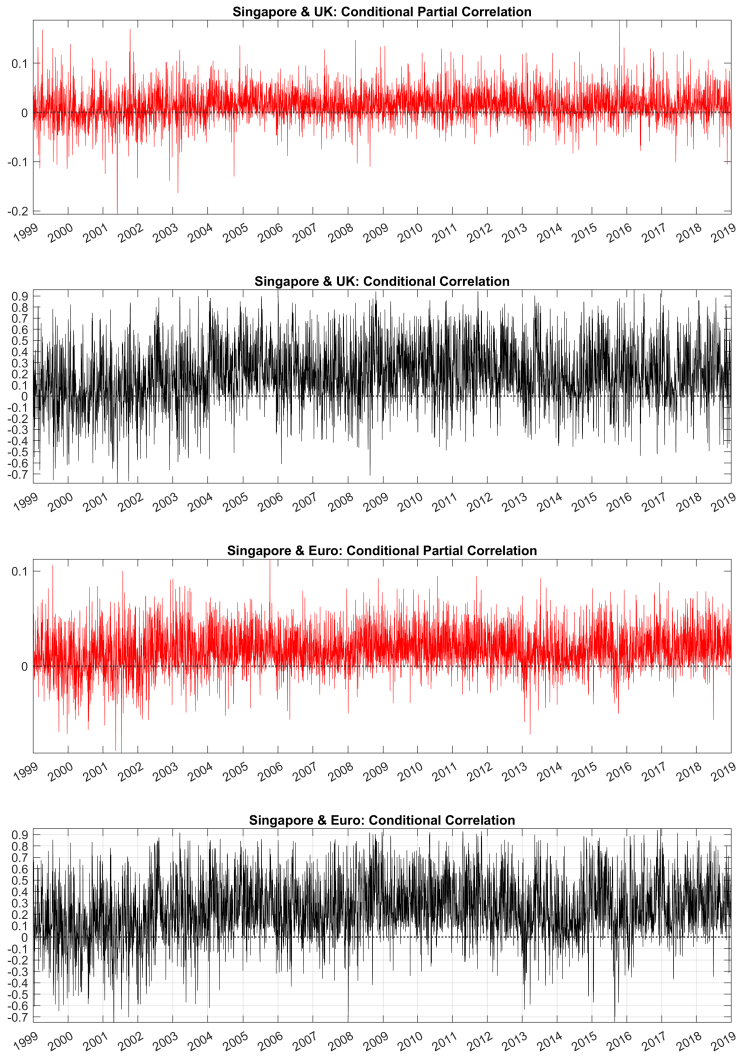


Figure 8: Dynamic Conditional (Partial) Correlations: Foreign Exchange Rates 2

Notes: The data encompasses a time span from January 4, 1999, to January 4, 2019. Volatility of the foreign exchange rate is quantified using the formula $\text{Volatility} = 100 \log \left(\frac{x_t}{x_{t-1}} \right)$, where x_t denotes the foreign exchange rate for the country under consideration at time t .

with the European sovereign debt crisis, where concerns surrounding several European countries' ability to refinance their government debt without the assistance of external parties loomed large. Given Singapore's role as a major financial hub, shifts in Europe's economic landscape would inevitably have ramifications on the Singaporean currency's volatility in relation to the Euro. On the other hand, the conditional correlations for both pairs, while oscillating, seem to maintain a tighter range, suggesting that when other variables are not controlled for, the co-movement in the foreign exchange volatility of these countries has some level of consistency.

5 Discussion and Interpretation

In this section, we explore the intricate nexus between conditional partial correlations and conditional independence, aiming to shed light on the complexities and potential pitfalls inherent in their interpretation. Additionally, we discuss empirical methodologies designed to address these challenges, thereby enhancing the robustness of our analysis.

Under the paradigm of multivariate normal distributions, zero partial correlations straightforwardly indicate conditional independence between variables. This straightforward interpretation stems from the complete characterization of the Gaussian distribution by its mean and covariance structure. However, this clarity diminishes in the context of non-normal distributions. Specifically, under non-Gaussian distributions, higher-order moments such as skewness and kurtosis can obscure the relationship, cautioning against a simplistic interpretation of zero partial correlations as indicative of conditional independence.

Building upon this foundational understanding, we next turn to two distinct facets of conditional independence within the realm of conditional partial correlations: the temporal and cross-sectional dimensions. Temporally, the presence of constant conditional partial correlations over successive time periods suggests that the conditional relationships between assets remain stable. Cross-sectionally, conditional independence manifests as zero conditional partial correlation between two assets i and j , conditioned on the remaining $N - 2$ assets and the information set \mathcal{F}_{t-1} . Notably, the temporal stability of these correlations could imply an invariant conditional dependence structure among assets over time, warranting its own line of inquiry.

The foregoing discussion assumes the absence of latent or unobservable variables, an assumption that, if violated, can complicate the interpretation of conditional independence. Unobserved factors can introduce various biases, including omitted variable and simultaneity bias. These biases can distort the estimated partial correlations, particularly if the latent variables correlate with the observed variables. Moreover, any synchronized shifts in conditional partial correlations across time could potentially signal the influence of unobservable common factors, necessitating further empirical scrutiny.

Addressing the presence of common factors in the dependence structure can be empirically

managed in multiple ways. For observable factors, one could analyze the residual dependence structure obtained from a model that explicitly incorporates these factors. For instance, consider the regression model

$$\ln \sigma_{it}^2 = \eta_0 + \eta_1 \ln \sigma_{\text{Mkt.}}^2 + \eta_2 \ln \sigma_{\text{Sec.}}^2 + y_{it},$$

where σ_{it}^2 represents measured volatility and $\sigma_{\text{Mkt.}}^2$ and $\sigma_{\text{Sec.}}^2$ stand for market and sector-specific volatilities, respectively. The residuals y_{it} from this model can then be incorporated into our primary model specification. When dealing with unobservable factors, alternative techniques such as linear principal components (Bai and Shi (2011); Fan, Liao, and Mincheva (2013)), common correlated effects (CCE) estimators (Pesaran (2006)), or Autoencoders (Rumelhart, McClelland, and PDP Research Group (1986); Baldi (2012)) can be employed to approximate these latent influences. However, the direct incorporation of these techniques into volatility models presents a set of challenges, primarily due to inherent non-linearities and specific model constraints. Thus, while these methods offer promising avenues for approximating latent influences, their application necessitates meticulous adaptation to the unique specifications of volatility models.

Having discussed the potential biases introduced by latent variables, it is also crucial to address another limitation inherent in our approach: its inability to capture tail-dependence. Our analytical model leverages conditional partial correlations to elucidate the conditional independence structure among financial assets. However, it is pertinent to note that this approach is not designed to capture tail-dependence, a crucial aspect of financial data especially relevant for extreme events. Conditional partial correlations primarily focus on linear relationships and are averaged measures derived from the entire distribution, thereby offering limited insight into the conditional independence structure in the tails of the distribution. For a more nuanced understanding of extreme co-movements, researchers might consider employing measures specifically tailored to capture conditional tail-dependence, although the development of such metrics remains an area for future exploration.

To conclude, it is imperative to distinguish between conditional independence—a statistical construct—and causal inference, which necessitates additional assumptions related to the data-generating process. A finding of conditional independence between variables i and j does not necessarily imply a lack of causal relationship; it merely suggests that, conditional on the other variables and past information, one variable does not offer predictive information about the other. Therefore, any causal claims would require further methodological considerations, perhaps employing different modeling frameworks designed explicitly for causal inference. This distinction underscores the need for rigorous empirical methodologies and cautious interpretation, particularly when navigating the multifaceted landscape of conditional independence within financial econometrics.

6 Conclusions

This paper contributes to financial econometrics by introducing a nuanced approach to volatility modeling, extending the scope beyond traditional multivariate frameworks. We have sought to address the limitations of existing methods, particularly their inability to capture intricate dependencies and conditional independence in financial returns, especially when the data exhibit non-normal characteristics such as asymmetry and leptokurtosis. Our method brings forth two main contributions.

First, we introduce a dynamic conditional framework employing precision matrices to assess volatility. Unlike traditional models like MGARCH and MSV, our approach focuses on the temporal evolution of these matrices, thereby enhancing our understanding of asset dependencies and market structures. Second, we offer a coherent Bayesian estimation procedure tailored for high-dimensional settings, mitigating the computational burdens often encountered in existing models. The proposed framework integrates elements from both DCC-GARCH and DC-MSV models, combining the adaptability of GARCH models with the Bayesian updating mechanisms inherent in MSV models. We can better approximate the underlying distributions and construct rank likelihoods for sparse precision matrices by employing a Nonparanormal method. Our empirical and simulation studies corroborate the efficacy of the proposed method in capturing the complexities of financial markets. While the method performs suboptimally under certain conditions, such as the CCC framework, it shows promise in more dynamic settings like DCC, mainly when the sample size is small. We acknowledge that this work is but one perspective in a rapidly evolving field, and while it offers a novel lens through which to study financial dependencies, it has its limitations. For instance, the trade-off between computational efficiency and accuracy remains an area that warrants further investigation.

Future research is encouraged to extend the current framework by incorporating latent factors into both the conditional dependence structures and the development of conditional tail-dependence as a development of partial correlation. Such extensions would build upon the foundational work presented here and offer new avenues for capturing more complex dependencies and behaviors in financial markets.

References

- AAS, K., C. CZADO, A. FRIGESSI, AND H. BAKKEN (2009): “Pair-copula constructions of multiple dependence,” *Insurance: Mathematics and economics*, 44(2), 182–198.
- AIELLI, G. P. (2013): “Dynamic conditional correlation: on properties and estimation,” *Journal of Business & Economic Statistics*, 31(3), 282–299.
- ANATOLYEV, S., AND V. PYRLIK (2022): “Copula shrinkage and portfolio allocation in ultra-high dimensions,” *Journal of Economic Dynamics and Control*, 143, 104508.

- ARDIA, D. (2008): "Bayesian estimation of the GARCH (1, 1) model with normal innovations," *Financial Risk Management with Bayesian Estimation of GARCH Models: Theory and Applications*, pp. 17–37.
- ASAI, M., AND M. MCALLEER (2009): "The structure of dynamic correlations in multivariate stochastic volatility models," *Journal of Econometrics*, 150(2), 182–192.
- (2011): "Alternative asymmetric stochastic volatility models," *Econometric Reviews*, 30(5), 548–564.
- BAI, J., AND S. SHI (2011): "Estimating high dimensional covariance matrices and its applications," *Annals of Economics and Finance*, pp. 199–215.
- BAILLIE, R. T., T. BOLLERSLEV, AND H. O. MIKKELSEN (1996): "Fractionally integrated generalized autoregressive conditional heteroskedasticity," *Journal of econometrics*, 74(1), 3–30.
- BALDI, P. (2012): "Autoencoders, unsupervised learning, and deep architectures," in *Proceedings of ICML workshop on unsupervised and transfer learning*, pp. 37–49. JMLR Workshop and Conference Proceedings.
- BARIGOZZI, M., AND C. BROWNLEES (2019): "Nets: Network estimation for time series," *Journal of Applied Econometrics*, 34(3), 347–364.
- BARIGOZZI, M., G. CAVALIERE, AND G. MORAMARCO (2022): "Factor network autoregressions," *arXiv preprint arXiv:2208.02925*.
- BARUNÍK, J., AND T. KŘEHLÍK (2018): "Measuring the frequency dynamics of financial connectedness and systemic risk," *Journal of Financial Econometrics*, 16(2), 271–296.
- BAUWENS, L., AND S. LAURENT (2005): "A new class of multivariate skew densities, with application to generalized autoregressive conditional heteroscedasticity models," *Journal of Business & Economic Statistics*, 23(3), 346–354.
- BHATTACHARYA, A., A. CHAKRABORTY, AND B. K. MALLICK (2016): "Fast sampling with Gaussian scale mixture priors in high-dimensional regression," *Biometrika*, p. asw042.
- BICKEL, P. J., AND E. LEVINA (2008a): "Covariance regularization by thresholding," *The Annals of Statistics*, 36(6), 2577–2604.
- (2008b): "Regularized estimation of large covariance matrices," *The Annals of Statistics*, 36(1), 199 – 227.
- BILLIO, M., M. CAPORIN, AND M. GOBBO (2003): "Block dynamic conditional correlation multivariate GARCH models," *Università di Venezia*.
- BILLIO, M., M. GETMANSKY, A. W. LO, AND L. PELIZZON (2012): "Econometric measures of connectedness and systemic risk in the finance and insurance sectors," *Journal of financial economics*, 104(3), 535–559.
- BOLLERSLEV, T. (1986): "Generalized autoregressive conditional heteroskedasticity," *Journal of econometrics*, 31(3), 307–327.
- (1990): "Modelling the coherence in short-run nominal exchange rates: a multivariate generalized ARCH model," *The review of economics and statistics*, pp. 498–505.
- BYKHOVSKAYA, A. (2022): "Time series approach to the evolution of networks: Prediction and esti-

- mation,” *Journal of Business & Economic Statistics*, 41(1), 170–183.
- CAI, T., AND W. LIU (2011): “Adaptive thresholding for sparse covariance matrix estimation,” *Journal of the American Statistical Association*, 106(494), 672–684.
- CHEN, C. W., R. GERLACH, AND M. K. SO (2006): “Comparison of nonnested asymmetric heteroskedastic models,” *Computational Statistics & Data Analysis*, 51(4), 2164–2178.
- CHEN, C. W., F.-C. LIU, AND M. K. SO (2008): “Heavy-tailed-distributed threshold stochastic volatility models in financial time series,” *Australian & New Zealand Journal of Statistics*, 50(1), 29–51.
- CHEN, C. W., AND M. K. SO (2006): “On a threshold heteroscedastic model,” *International Journal of Forecasting*, 22(1), 73–89.
- CHEN, J., D. LI, AND O. LINTON (2019): “A new semiparametric estimation approach for large dynamic covariance matrices with multiple conditioning variables,” *Journal of Econometrics*, 212(1), 155–176.
- CHEN, Z., AND C. LENG (2016): “Dynamic covariance models,” *Journal of the American Statistical Association*, 111(515), 1196–1207.
- CHIANG, T. C., C. W. CHEN, AND M. K. SO (2007): “Asymmetric return and volatility responses to composite news from stock markets,” *Multinational Finance Journal*, 11(3/4), 179–210.
- DAHLHAUS, R. (2000): “Graphical interaction models for multivariate time series,” *Metrika*, 51, 157–172.
- DIEBOLD, F. X., AND K. YILMAZ (2014): “On the network topology of variance decompositions: Measuring the connectedness of financial firms,” *Journal of econometrics*, 182(1), 119–134.
- (2015): *Financial and macroeconomic connectedness: A network approach to measurement and monitoring*. Oxford University Press, USA.
- DOBRA, A., AND A. LENKOSKI (2011): “Copula Gaussian graphical models and their application to modeling functional disability data,” *The Annals of Applied Statistics*, 5(2A), 969 – 993.
- EICHLER, M. (2007): “Granger causality and path diagrams for multivariate time series,” *Journal of Econometrics*, 137(2), 334–353.
- ENGLE, R. F. (1982): “Autoregressive conditional heteroscedasticity with estimates of the variance of United Kingdom inflation,” *Econometrica: Journal of the econometric society*, pp. 987–1007.
- (2002): “Dynamic Conditional Correlation: A Simple Class of Multivariate Generalized Autoregressive Conditional Heteroskedasticity Models,” *Journal of Business & Economic Statistics*, 20(3), 339–350.
- ENGLE, R. F., AND K. F. KRONER (1995): “Multivariate Simultaneous Generalized Arch,” *Econometric Theory*, 11(1), 122–150.
- ENGLE, R. F., O. LEDOIT, AND M. WOLF (2019): “Large Dynamic Covariance Matrices,” *Journal of Business & Economic Statistics*, 37(2), 363–375.
- FAN, J., Y. LIAO, AND M. MINCHEVA (2013): “Large covariance estimation by thresholding principal orthogonal complements,” *Journal of the Royal Statistical Society Series B: Statistical Methodology*, 75(4), 603–680.

- FERNÁNDEZ, C., AND M. F. STEEL (1998): "On Bayesian modeling of fat tails and skewness," *Journal of the American Statistical Association*, 93(441), 359–371.
- FIORUCI, J. A., R. S. EHLERS, AND M. G. ANDRADE FILHO (2014): "Bayesian multivariate GARCH models with dynamic correlations and asymmetric error distributions," *Journal of Applied Statistics*, 41(2), 320–331.
- GIANNONE, D., M. LENZA, AND G. E. PRIMICERI (2021): "Economic predictions with big data: The illusion of sparsity," *Econometrica*, 89(5), 2409–2437.
- HÄRDLE, W. K., W. WANG, AND L. YU (2016): "Tenet: Tail-event driven network risk," *Journal of Econometrics*, 192(2), 499–513.
- HARVEY, A., E. RUIZ, AND N. SHEPHARD (1994): "Multivariate stochastic variance models," *The Review of Economic Studies*, 61(2), 247–264.
- HARVEY, A. C., AND N. SHEPHARD (1996): "Estimation of an asymmetric stochastic volatility model for asset returns," *Journal of Business & Economic Statistics*, 14(4), 429–434.
- HAUTSCH, N., J. SCHAUMBURG, AND M. SCHIENLE (2015): "Financial network systemic risk contributions," *Review of Finance*, 19(2), 685–738.
- HOFF, P. D. (2007): "Extending the rank likelihood for semiparametric copula estimation," *The Annals of Applied Statistics*, 1(1), 265 – 283.
- ISHIHARA, T., Y. OMORI, AND M. ASAI (2016): "Matrix exponential stochastic volatility with cross leverage," *Computational Statistics & Data Analysis*, 100, 331–350.
- KAWAKATSU, H. (2006): "Matrix exponential GARCH," *Journal of Econometrics*, 134(1), 95–128.
- KIM, J.-M., AND H. JUNG (2016): "Linear time-varying regression with Copula–DCC–GARCH models for volatility," *Economics Letters*, 145, 262–265.
- LEDOIT, O., AND M. WOLF (2003): "Improved estimation of the covariance matrix of stock returns with an application to portfolio selection," *Journal of Empirical Finance*, 10(5), 603–621.
- (2004a): "Honey, I shrunk the sample covariance matrix," *Journal of Portfolio Management*, 30(1), 110–119.
- (2004b): "A well-conditioned estimator for large-dimensional covariance matrices," *Journal of Multivariate Analysis*, 88(2), 365–411.
- (2012): "Nonlinear shrinkage estimation of large-dimensional covariance matrices," *The Annals of Statistics*, 40(2), 1024–1060.
- (2017): "Nonlinear Shrinkage of the Covariance Matrix for Portfolio Selection: Markowitz Meets Goldilocks," *The Review of Financial Studies*, 30(12), 4349–4388.
- (2020): "Analytical nonlinear shrinkage of large-dimensional covariance matrices," *The Annals of Statistics*, 48(5), 3043–3065.
- (2022): "Quadratic shrinkage for large covariance matrices," *Bernoulli*, 28(3), 1519–1547.
- LI, Z. R., AND T. H. MCCORMICK (2019): "An expectation conditional maximization approach for Gaussian graphical models," *Journal of Computational and Graphical Statistics*, 28(4), 767–777.
- LIU, H., F. HAN, M. YUAN, J. LAFFERTY, AND L. WASSERMAN (2012): "High-dimensional semi-

- parametric Gaussian copula graphical models," *The Annals of Statistics*, 40(4), 2293 – 2326.
- LIU, H., J. LAFFERTY, AND L. WASSERMAN (2009): "The nonparanormal: Semiparametric estimation of high dimensional undirected graphs," *Journal of Machine Learning Research*, 10(10).
- MLIKOTA, M. (2022): "Cross-sectional dynamics under network structure: Theory and macroeconomic applications," *arXiv preprint arXiv:2211.13610*.
- MOHAMMADI, A., F. ABEGAZ, E. HEUVEL, AND E. C. WIT (2017): "Bayesian modelling of Dupuytren disease by using Gaussian copula graphical models," *Journal of the Royal Statistical Society Series C: Applied Statistics*, 66(3), 629–645.
- MOHAMMADI, A., AND E. C. WIT (2015): "Bayesian Structure Learning in Sparse Gaussian Graphical Models," *Bayesian Analysis*, 10(1), 109 – 138.
- MULGRAVE, J. J., AND S. GHOSAL (2020): "Bayesian Inference in Nonparanormal Graphical Models," *Bayesian Analysis*, 15(2), 449 – 475.
- (2022): "Regression-based Bayesian estimation and structure learning for nonparanormal graphical models," *Statistical Analysis and Data Mining: The ASA Data Science Journal*, 15(5), 611–629.
- (2023): "Bayesian analysis of nonparanormal graphical models using rank-likelihood," *Journal of Statistical Planning and Inference*, 222, 195–208.
- MÜLLER, D., AND C. CZADO (2019a): "Dependence modelling in ultra high dimensions with vine copulas and the Graphical Lasso," *Computational Statistics & Data Analysis*, 137, 211–232.
- (2019b): "Selection of sparse vine copulas in high dimensions with the lasso," *Statistics and Computing*, 29(2), 269–287.
- NAKAJIMA, J., AND Y. OMORI (2012): "Stochastic volatility model with leverage and asymmetrically heavy-tailed error using GH skew Student's t-distribution," *Computational Statistics & Data Analysis*, 56(11), 3690–3704.
- NARD, G. D., R. F. ENGLE, O. LEDOIT, AND M. WOLF (2022): "Large dynamic covariance matrices: Enhancements based on intraday-data," *Journal of Banking & Finance*, 138, 106426.
- NELSON, D. B. (1991): "Conditional heteroskedasticity in asset returns: A new approach," *Econometrica: Journal of the econometric society*, pp. 347–370.
- NEVILLE, S. E., J. T. ORMEROD, AND M. P. WAND (2014): "Mean field variational Bayes for continuous sparse signal shrinkage: Pitfalls and remedies," *Electronic Journal of Statistics*, 8(1), 1113 – 1151.
- OH, D. H., AND A. J. PATTON (2016): "High-dimensional copula-based distributions with mixed frequency data," *Journal of Econometrics*, 193(2), 349–366.
- (2017): "Modeling dependence in high dimensions with factor copulas," *Journal of Business & Economic Statistics*, 35(1), 139–154.
- (2023): "Dynamic factor copula models with estimated cluster assignments," *Journal of Econometrics*.
- PAKEL, C., N. SHEPHARD, K. SHEPPARD, AND R. F. ENGLE (2021): "Fitting Vast Dimensional Time-Varying Covariance Models," *Journal of Business & Economic Statistics*, 39(3), 652–668.

- PATTON, A. J. (2009): “Copula-based models for financial time series,” in *Handbook of financial time series*, pp. 767–785. Springer.
- PESARAN, M. H. (2006): “Estimation and inference in large heterogeneous panels with a multifactor error structure,” *Econometrica*, 74(4), 967–1012.
- PITT, M., D. CHAN, AND R. KOHN (2006): “Efficient Bayesian inference for Gaussian copula regression models,” *Biometrika*, 93(3), 537–554.
- POIGNARD, B., AND M. ASAI (2023): “High-dimensional sparse multivariate stochastic volatility models,” *Journal of Time Series Analysis*, 44(1), 4–22.
- ROTHMAN, A. J., E. LEVINA, AND J. ZHU (2009): “Generalized thresholding of large covariance matrices,” *Journal of the American Statistical Association*, 104(485), 177–186.
- RUE, H., AND L. HELD (2005): *Gaussian Markov random fields: theory and applications*. CRC press.
- RUMELHART, D. E., J. L. MCCLELLAND, AND C. PDP RESEARCH GROUP (1986): *Parallel distributed processing: Explorations in the microstructure of cognition, Vol. 1: Foundations*. MIT press.
- SENTANA, E. (1995): “Quadratic ARCH models,” *The Review of Economic Studies*, 62(4), 639–661.
- SO, M. K., C. W. CHEN, J.-Y. LEE, AND Y.-P. CHANG (2008): “An empirical evaluation of fat-tailed distributions in modeling financial time series,” *Mathematics and Computers in Simulation*, 77(1), 96–108.
- SO, M. K., AND I. W. YIP (2012): “Multivariate GARCH models with correlation clustering,” *Journal of Forecasting*, 31(5), 443–468.
- TSE, Y. K., AND A. K. C. TSUI (2002): “A Multivariate Generalized Autoregressive Conditional Heteroscedasticity Model with Time-Varying Correlations,” *Journal of Business & Economic Statistics*, 20(3), 351–362.
- WAGNER, N., AND T. A. MARSH (2005): “Measuring tail thickness under GARCH and an application to extreme exchange rate changes,” *Journal of Empirical Finance*, 12(1), 165–185.

A Appendix

A.1 Algorithm 1: Sampling the transformed standardized residuals

Algorithm 1 Sample $\mathbf{Z} \sim \mathcal{N}(\mathbf{0}, \mathbf{S}^{-1})$

```

1: for i=1:n do
2:   for r=1:T do
3:     if r = 1 then
4:        $z_{i,t_0} = -\infty$ 
5:     else
6:        $z_{i,t_{r-1}} = u_{i,t_{r-1}}$ 
7:     end if
8:     if r = T then
9:        $z_{i,t_{T+1}} = \infty$ 
10:    else
11:       $z_{i,t_{r+1}} = u_{i,t_{r+1}}$ 
12:    end if
13:    Compute  $\mu_{t_r,i} = -\psi_{i,i}^{-1} \Psi_{n \setminus i,i} \mathbf{u}_{n \setminus i,t_r}$ 
14:    Compute  $\sigma_i^2 = \psi_{i,i}^{-1}$ 
15:    Sample  $z_{i,t_r} \sim \mathcal{T}\mathcal{N}(\mu_{t_r,i}, \sigma_i^2; z_{i,t_{r-1}} < z_{i,t_r} < z_{i,t_{r+1}})$ 
16:  end for
17: end for

```

A.2 Algorithm 2: Sampling the sparse unconditional precision matrix

Expanding upon the variation in the horseshoe prior specification, as articulated in Model III by Neville, Ormerod, and Wand (2014), and Mulgrave and Ghosal (2022, 2023) set forth a series of prior distributions for β in Equation (2.8). For $j = 1, 2, \dots, N$ and $i = j + 1, j + 2, \dots, N$, the priors are formulated as follows:

$$\begin{aligned}
\mathbf{Z}_j | \mathbf{Z}_{i>j}, \beta_{i>j} \sigma_j^2 &\sim \mathcal{N}(\mathbf{Z}_{i>j} \beta_{i>j}, \sigma_j^2 \mathbb{I}), \\
\beta_{i>j} | \lambda_j^2, \mathbf{b}_{i>j}, \sigma_j^2 &\sim \mathcal{N}\left(\mathbf{0}, \frac{\sigma_j^2 \mathbf{b}_{i>j} c^2 \lambda_j^2}{N^2 i}\right), \\
\lambda_j^2 | a_j &\sim \mathcal{IG}\left(\frac{1}{2}, \frac{1}{a_j}\right), \quad a_j \sim \mathcal{IG}\left(\frac{1}{2}, 1\right), \\
\mathbf{b}_{i>j} | h_{i>j} &\sim \mathcal{IG}\left(\frac{1}{2}, \frac{1}{h_{i>j}}\right), \quad h_{i>j} \sim \mathcal{IG}\left(\frac{1}{2}, 1\right), \\
\sigma_j^2 &\sim \mathcal{IG}(0.01, 0.01),
\end{aligned} \tag{A.1}$$

where \mathcal{IG} stands for the inverse gamma distribution, and σ_j^2 is chosen to be a diffuse prior. Given these priors, the posterior distribution for $\beta_{i>j}$ can be derived. The probability density in Equation (2.8) is:

$$\mathcal{L}(\mathbf{Z}_j | \mathbf{Z}_{i>j}\beta_{i>j}, \sigma_j^2) \propto \exp \left\{ -\frac{1}{2\sigma_j^2} (\mathbf{Z}_j - \mathbf{Z}_{i>j}\beta_{i>j})' (\mathbf{Z}_j - \mathbf{Z}_{i>j}\beta_{i>j}) \right\}. \quad (\text{A.2})$$

Coupling this with the prior distribution for $\beta_{i>j}$ in Equation (A.1), defined as:

$$p(\beta_{i>j} | \lambda_j^2, \mathbf{b}_{i>j}, \sigma_j^2) \propto \exp \left\{ -\frac{N^2 i}{2\sigma_j^2 \mathbf{b}_{i>j} c^2 \lambda_j^2} \beta'_{i>j} \beta_{i>j} \right\}. \quad (\text{A.3})$$

Then, from Equations (A.2) and (A.3), the resulting posterior distribution is:

$$\begin{aligned} p(\beta_{i>j} | \mathbf{Z}_j, \mathbf{Z}_{i>j}, \lambda_j^2, b_{i>j}, \sigma_j^2) &\propto \mathcal{L}(\mathbf{Z}_j | \mathbf{Z}_{i>j}\beta_{i>j}, \sigma_j^2) \cdot p(\beta_{i>j} | \lambda_j^2, \mathbf{b}_{i>j}, \sigma_j^2) \\ &\propto \exp \left\{ -\frac{1}{2\sigma_j^2} (\mathbf{Z}_j - \mathbf{Z}_{i>j}\beta_{i>j})' (\mathbf{Z}_j - \mathbf{Z}_{i>j}\beta_{i>j}) \right. \\ &\quad \left. - \frac{N^2 i}{2\sigma_j^2 \mathbf{b}_{i>j} c^2 \lambda_j^2} \beta'_{i>j} \beta_{i>j} \right\} \\ &\propto \exp \left\{ -\frac{1}{2\sigma_j^2} \beta'_{i>j} \left(\mathbf{Z}'_{i>j} \mathbf{Z}_{i>j} + \text{diag} \left\{ \frac{N^2 i}{2\sigma_j^2 \mathbf{b}_{i>j} c^2 \lambda_j^2} \right\} \right) \beta_{i>j} \right. \\ &\quad \left. + \frac{1}{\sigma_j^2} \beta'_{i>j} \mathbf{Z}'_{i>j} \mathbf{Z}_j \right\}. \end{aligned}$$

The distribution exhibits Gaussian properties with mean mean $\mathbf{A}^{-1} \mathbf{Z}'_{i>j} \mathbf{Z}_j$ and covariance $\sigma_j^2 \mathbf{A}^{-1}$, where $\mathbf{A} = \mathbf{Z}'_{i>j} \mathbf{Z}_{i>j} + \text{diag} \left\{ \frac{N^2 i}{2\sigma_j^2 \mathbf{b}_{i>j} c^2 \lambda_j^2} \right\}$ and we can write it as

$$\beta_{i>j} | \lambda_j^2, \mathbf{b}_{i>j}, \sigma_j^2 \sim \mathcal{N}(\mathbf{A}^{-1} \mathbf{Z}'_{i>j} \mathbf{Z}_j, \sigma_j^2 \mathbf{A}^{-1}). \quad (\text{A.4})$$

To ameliorate computational burden, particularly for large N , we also adopts an exact sampling algorithm tailored for Gaussian priors, incorporating data augmentation as outlined in Bhattacharya, Chakraborty, and Mallick (2016). Algorithm 2 elaborates this methodology.

Algorithm 2 Sample sparse unconditional precision matrix Ω

- 1: Given initial hyperparameters for λ_j^2 , $\mathbf{b}_{i>j}$, σ_j^2 , and c ,
 - 2: **for** $j = 1 : N - 1$ **do**
 - 3: Partition $\mathbf{Z}_{i>j}$ and \mathbf{Z}_j .
 - 4: Compute $\mathbf{D} = \text{diag} \left\{ \frac{\lambda_j^2 \mathbf{b}_{i>j} c^2}{N^2 i} \frac{1}{\sigma_j^2} \right\}$ for $i > j$, $\Phi = \sqrt{\sigma_j^2} \mathbf{Z}_{i>j}$, and $\mathbf{a} = \sqrt{\sigma_j^2} \mathbf{Z}_j$.
 - 5: Sample $\phi \sim \mathcal{N}(0, \mathbf{D})$, $v = \Phi\phi + \mathcal{N}(0, \mathbb{I})$ and solve for w in $(\Phi\mathbf{D}\Phi + \mathbb{I})w = (\mathbf{a} - v)$.
 - 6: Given ϕ , \mathbf{D} , Φ , and w , sample $\beta_{i>j} = u + \mathbf{D}\Phi'w$.
 - 7: Sample $\lambda_j^2 \sim \mathcal{IG} \left(\frac{|i>j|}{2} + \frac{1}{2}, K_1 \right)$, where $K_1 = \frac{1}{2} \beta'_{i>j} \text{diag} \left\{ \frac{N^2 i}{\sigma_j^2 \mathbf{b}_{i>j} c^2} \right\} \beta_{i>j} + \frac{1}{a_j}$ for $i > j$.
 - 8: Sample $a_j \sim \mathcal{IG} (1, 1 + \lambda_j^{-2})$.
 - 9: Sample $\mathbf{b}_{i>j} \sim \mathcal{IG} (1, K_2)$, where $K_2 = \frac{N^2 i}{2\sigma_j^2 \lambda_j^2 c^2} \beta_{i>j} + \frac{1}{h_{i>j}}$ for $i > j$.
 - 10: Sample $h_{i>j} \sim \mathcal{IG} (1, 1 + \frac{1}{\mathbf{b}_{i>j}})$.
 - 11: Sample $\sigma_j^2 \sim \mathcal{IG} \left(\frac{T+|i>j|}{2} + 0.01, K_3 \right)$, where $K_3 = \frac{1}{2} \|\mathbf{Z}_j - \mathbf{Z}_{i>j} \beta_{i>j}\|^2 + \frac{1}{2} \beta'_{i>j} \text{diag} \left\{ \frac{N^2 i}{\lambda_j^2 \mathbf{b}_{i>j} c^2} \right\} \beta_{i>j} + 0.01$ for $i > j$.
 - 12: Update $L_{jj} = \sqrt{\sigma_j^2}$ and $L_{ij} = -\beta_{i>j}/L_{jj}$ for $i > j$.
 - 13: **end for**
 - 14: Sample $\sigma_N^2 \sim \mathcal{IG} \left(\frac{N}{2} + 0.01, K_4 \right)$, where $K_4 = 0.01 + \frac{1}{2} \|\mathbf{Z}_N\|^2$.
 - 15: Update $L_{NN} = \sqrt{\sigma_N^2}$.
 - 16: Compute $\Omega = \mathbf{L}\mathbf{L}'$.
-

A.3 Algorithm 3: Nonparanormal Bayesian Dynamic Partial Correlation

To efficiently explore the parameter space, an optimization problem targeting the log-posterior distribution is initially solved to acquire starting parameters. If the resultant Hessian matrix is not positive-definite, an adaptive Metropolis-Hastings Markov Chain Monte Carlo (MH-MCMC) strategy is employed to construct the proposal distribution. This approach entails an initial ‘pilot run’ for sample generation, succeeded by an adaptation phase during which the proposal distribution is refined based on the empirical covariance matrix of the observed samples. Concurrently, the step-size of the proposal distribution is adjusted to regulate the acceptance rate within an optimal range of 20% to 50%. The adapted proposal distribution and step-size are then utilized in the subsequent main MCMC run, as detailed in Algorithm 3.

Algorithm 3 Nonparanormal Bayesian Dynamic Partial Correlation – GARCH(1,1)

```

1: for 1=1:#Simulation do
2:   Choose initial parameter values  $\Theta_0 = w_1, \theta_{10}, \theta_{11}, \dots, w_N, \theta_{N0}, \theta_{N1}, a, b$  for the model
3:   Compute Log-Rank Likelihood:
4:   Compute standardized residuals  $\mathbf{U}$ .
5:   Compute transformed standardized residuals  $\mathbf{Z}$  from Algorithm 1.
6:   Sample regularized unconditional precision matrix  $\Omega$  from Algorithm 2.
7:   Given  $\mathbf{H}_1$  and  $\mathbf{Q}_1$  based on  $\Omega$  at  $t = 1$ ,
8:   for  $t > 1$  do
9:     Sample  $\Xi_t \sim \mathcal{W}((\mathbb{I} + \mathbf{Z}'_{t-1}\mathbf{Z}_{t-1})^{-1}, 3 + T)$ .
10:    Update  $\mathbf{Q}$ :  $\mathbf{Q}_t = (1 - a - b)\Omega + a\Xi_t + b\mathbf{Q}_{t-1}$ .
11:    Update Diagonal Elements of  $\mathbf{H}_t$  as specified in (2.3).
12:    Update Off-Diagonal Elements of  $\mathbf{H}_t$ : Compute  $\mathbf{S}_t = \mathbf{Q}_t / \sqrt{\text{diag}\{\mathbf{Q}_t\}\text{diag}\{\mathbf{Q}_t\}'}$ ,
       $\mathbf{R}_t = \mathbf{S}_t^{-1}$ , and  $\mathbf{H}_t = \mathbf{R}_t / \sqrt{\text{diag}\{\mathbf{H}_t\}\text{diag}\{\mathbf{H}_t\}'}$ .
13:    Save the current  $\mathbf{S}_t$  and  $\mathbf{H}_t$  for later use.
14:    Update Log-Rank Likelihood based on the error distribution specified in (2.9).
15:   end for
16:   Compute Log-Posterior for  $\mathbf{S}_t$  from the found Log-Rank Likelihood and Log Prior for
       $\Theta_t$  as specified in Section 2.4.
17:   Compute Log-Posterior for  $\Theta_t$  from the Log-Posterior for  $\mathbf{S}_t$  and Log-Jacobian for  $\Theta_t$ .
18:   Given Log-Posterior, generate a new parameter set by perturbing the current parameter
      set and decide whether to accept the new parameter set based on the Metropolis criterion.
19: end for
20: From the acquired MH-MCMC samples of  $\mathbf{S}_t$  to compute the inverse-correlation matrix  $\Psi_t$ 
      as Equation (2.6).

```

In high-dimensional settings where the number of variables exceeds 25, the computational burden of estimating more than 100 parameters becomes prohibitive. To ameliorate this, we adopt an approach akin to that delineated in Pakel, Shephard, Sheppard, and Engle (2021). Specifically, initial parameters are derived from optimizing univariate GARCH models for each variable, rather than through a joint fit under the log-posterior distribution. Subsequent analysis focuses solely on parameters pertinent to conditional partial correlation matrices and associated error distributions. This strategy effectively minimizes the number of jointly estimated parameters and the requisite pilot simulations for establishing a viable proposal distribution. Nonetheless, it introduces complexities stemming from the approximations inherent in the initial parameters. An alternative strategy for approximating the full posterior distribution involves Bayesian variational inference; however, this avenue is not explored in the present study.

B Additional Empirical Results

B.1 Foreign Stock Price Indexes

The figure presented below delineates the volatility characteristics of the foreign stock indices examined in the empirical application, as articulated in Section 4.1.

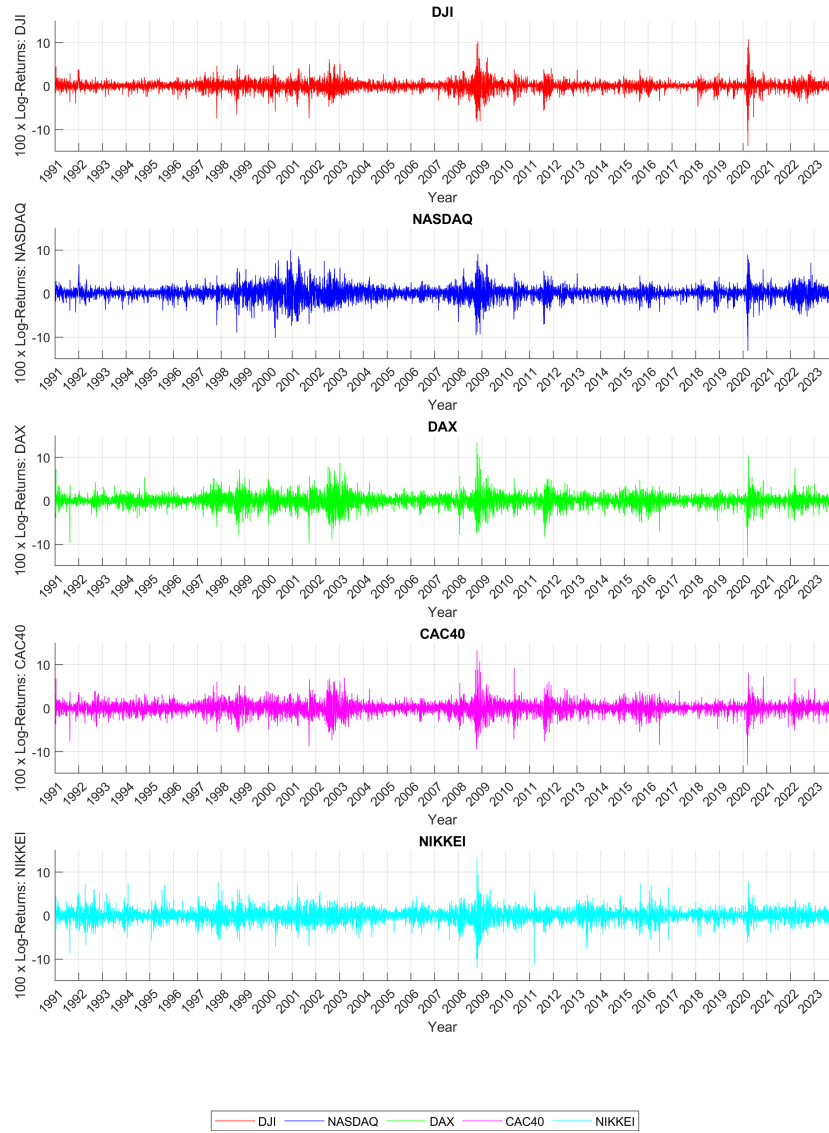


Figure A1: Stock Index Volatilities: DJI, NASDAQ, DAX, CAC40, NIKKEI

Notes: The dataset has been sourced from Google Finance, spanning the period from January 4, 1991, to August 31, 2023. The measure for volatility is calculated using the formula: $\text{Volatility} = 100 \log(p_t/p_{t-1})$, where p_t represents the closing price of the respective stock index. The abbreviations for the stock indexes are as follows: DJI denotes the Dow Jones Industrial Average, NASDAQ signifies the National Association of Securities Dealers Automated Quotations, DAX stands for Deutscher Aktienindex, CAC40 is an acronym for Cotation AssistÃ©e en Continu 40, and NIKKEI represents the Nikkei 225 Stock Average.

B.2 S&P 100

The subsequent figures delineate the conditional and partial correlation coefficients associated with the selected firms within each respective GICS sector.

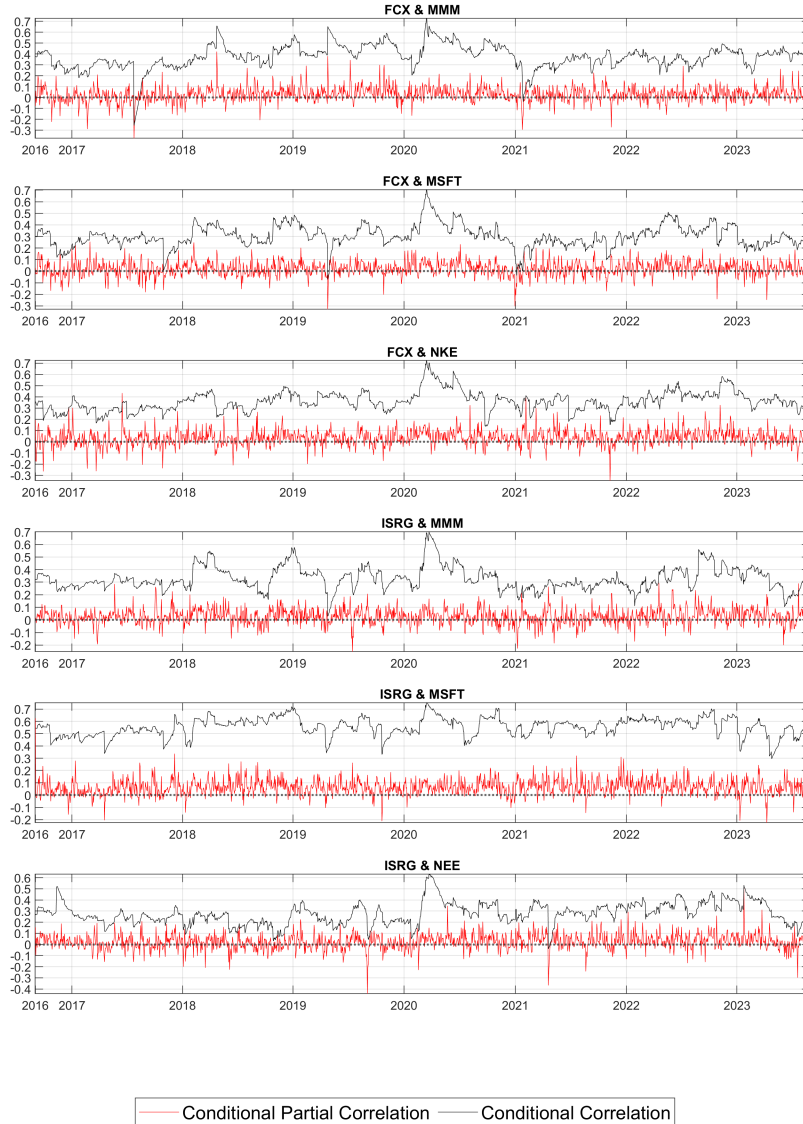


Figure A2: Dynamic Conditional (Partial) Correlations: High-Degree S&P100 Stocks 1

Notes: The figure describes the dynamic conditional correlations and dynamic conditional partial correlations among stock price volatilities for sectors characterized by a high degree of unconditional dependence. Stock ticker symbols corresponding to each sector are delineated as follows: Materials (FCX), Health Care (ISRG), Industrials (MMM), Information Technology (MSFT), Utilities (NEE), Communication Services (NFLX), Consumer Discretionary (NKE), Financials (SPG), Consumer Staples (WMT), and Energy (XOM). A comprehensive list of associated stock tickers can be found in Appendix C. To enhance visual representation, the dynamic conditional partial correlations have been scaled by a factor of 10.

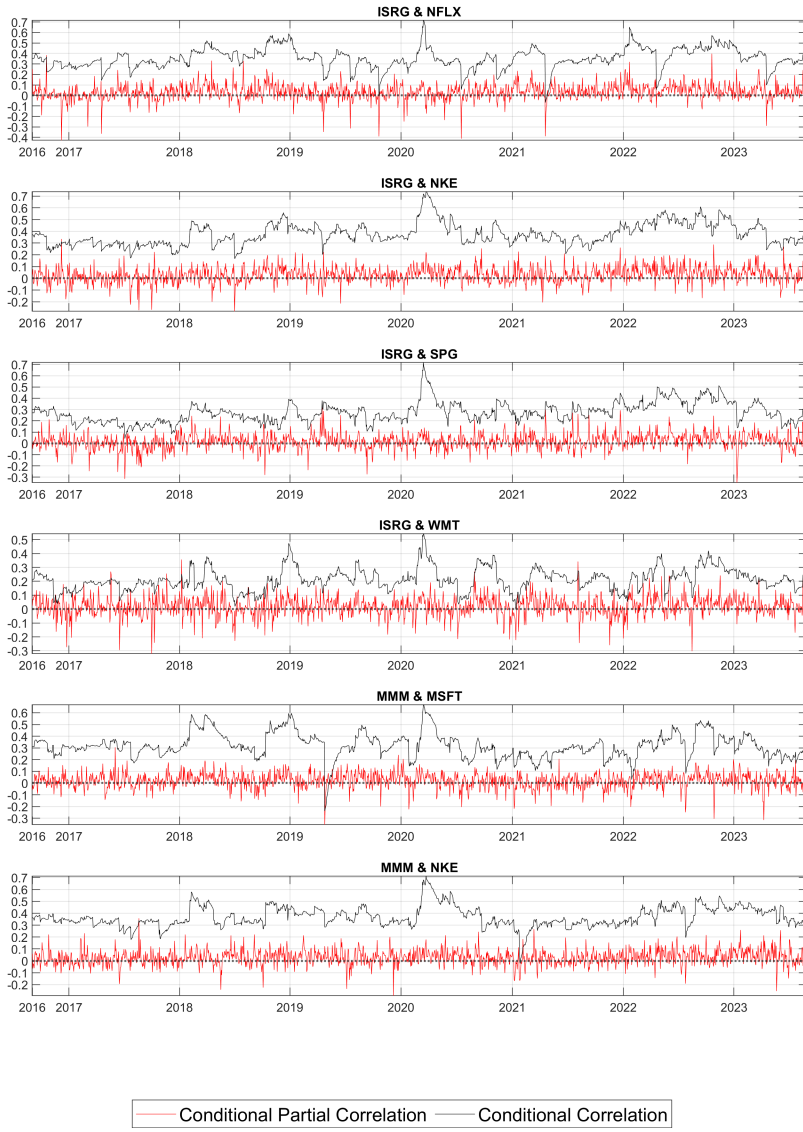


Figure A3: Dynamic Conditional (Partial) Correlations: High-Degree S&P100 Stocks 2

Notes: The figure describes the dynamic conditional correlations and dynamic conditional partial correlations among stock price volatilities for sectors characterized by a high degree of unconditional dependence. Stock ticker symbols corresponding to each sector are delineated as follows: Materials (FCX), Health Care (ISRG), Industrials (MMM), Information Technology (MSFT), Utilities (NEE), Communication Services (NFLX), Consumer Discretionary (NKE), Financials (SPG), Consumer Staples (WMT), and Energy (XOM). A comprehensive list of associated stock tickers can be found in Appendix C. To enhance visual representation, the dynamic conditional partial correlations have been scaled by a factor of 10.

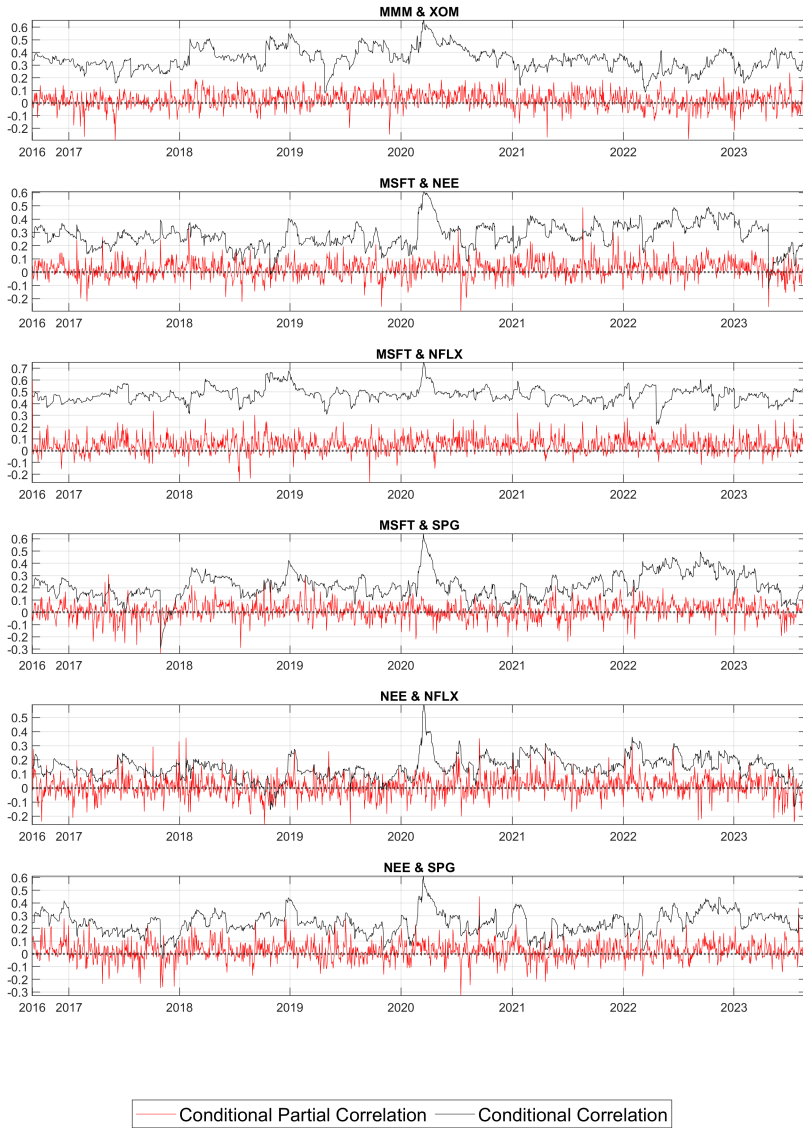


Figure A4: Dynamic Conditional (Partial) Correlations: High-Degree S&P100 Stocks 3

Notes: The figure describes the dynamic conditional correlations and dynamic conditional partial correlations among stock price volatilities for sectors characterized by a high degree of unconditional dependence. Stock ticker symbols corresponding to each sector are delineated as follows: Materials (FCX), Health Care (ISRG), Industrials (MMM), Information Technology (MSFT), Utilities (NEE), Communication Services (NFLX), Consumer Discretionary (NKE), Financials (SPG), Consumer Staples (WMT), and Energy (XOM). A comprehensive list of associated stock tickers can be found in Appendix C. To enhance visual representation, the dynamic conditional partial correlations have been scaled by a factor of 10.

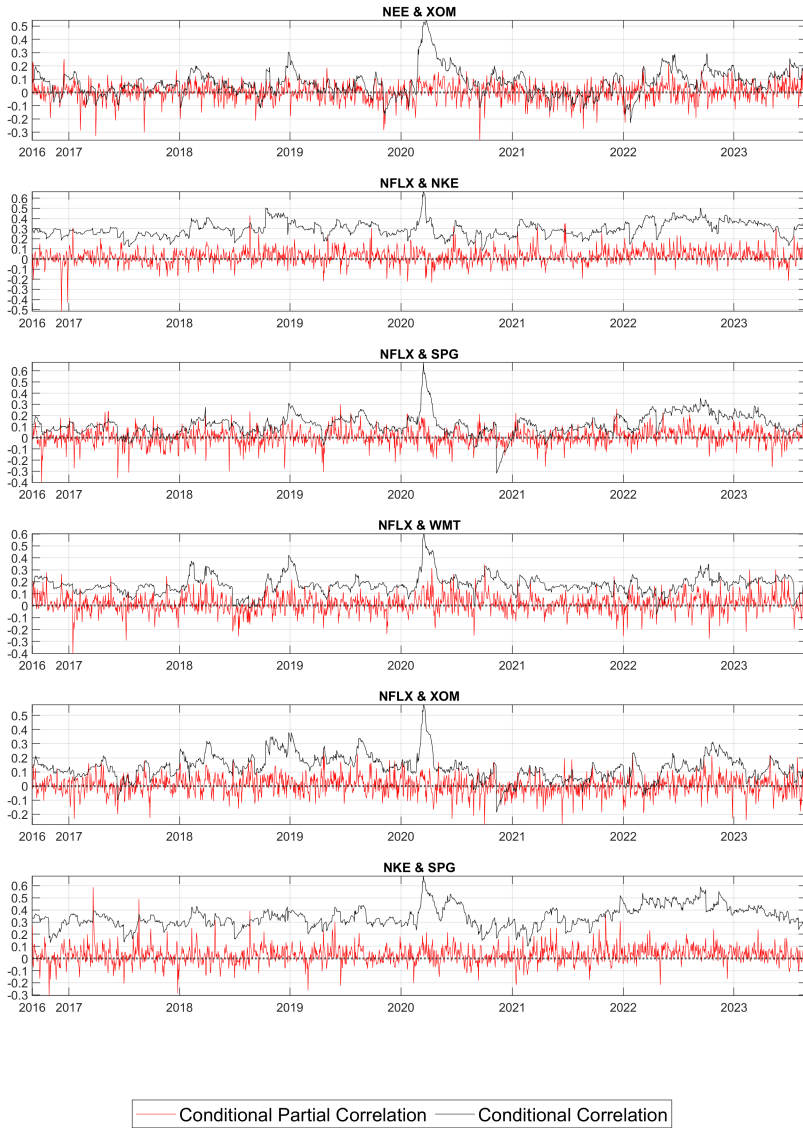


Figure A5: Dynamic Conditional (Partial) Correlations: High-Degree S&P100 Stocks 4

Notes: The figure describes the dynamic conditional correlations and dynamic conditional partial correlations among stock price volatilities for sectors characterized by a high degree of unconditional dependence. Stock ticker symbols corresponding to each sector are delineated as follows: Materials (FCX), Health Care (ISRG), Industrials (MMM), Information Technology (MSFT), Utilities (NEE), Communication Services (NFLX), Consumer Discretionary (NKE), Financials (SPG), Consumer Staples (WMT), and Energy (XOM). A comprehensive list of associated stock tickers can be found in Appendix C. To enhance visual representation, the dynamic conditional partial correlations have been scaled by a factor of 10.

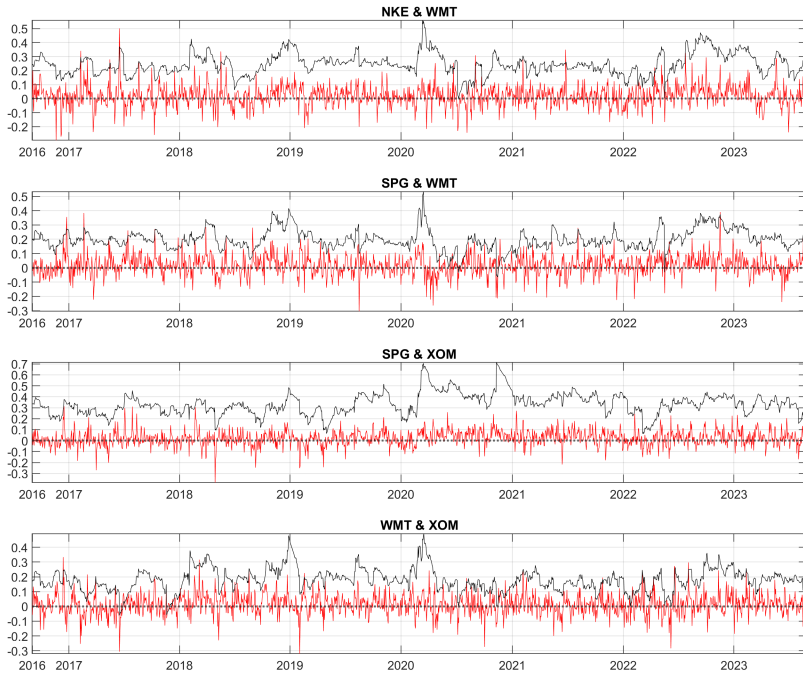


Figure A6: Dynamic Conditional (Partial) Correlations: High-Degree S&P100 Stocks 5

Notes: The figure describes the dynamic conditional correlations and dynamic conditional partial correlations among stock price volatilities for sectors characterized by a high degree of unconditional dependence. Stock ticker symbols corresponding to each sector are delineated as follows: Materials (FCX), Health Care (ISRG), Industrials (MMM), Information Technology (MSFT), Utilities (NEE), Communication Services (NFLX), Consumer Discretionary (NKE), Financials (SPG), Consumer Staples (WMT), and Energy (XOM). A comprehensive list of associated stock tickers can be found in Appendix C. To enhance visual representation, the dynamic conditional partial correlations have been scaled by a factor of 10.

B.3 Foreign Exchange Rates

The subsequent figures present a comprehensive depiction of the dynamic conditional partial correlations pertaining to foreign exchange rate volatility in the context of Singapore.

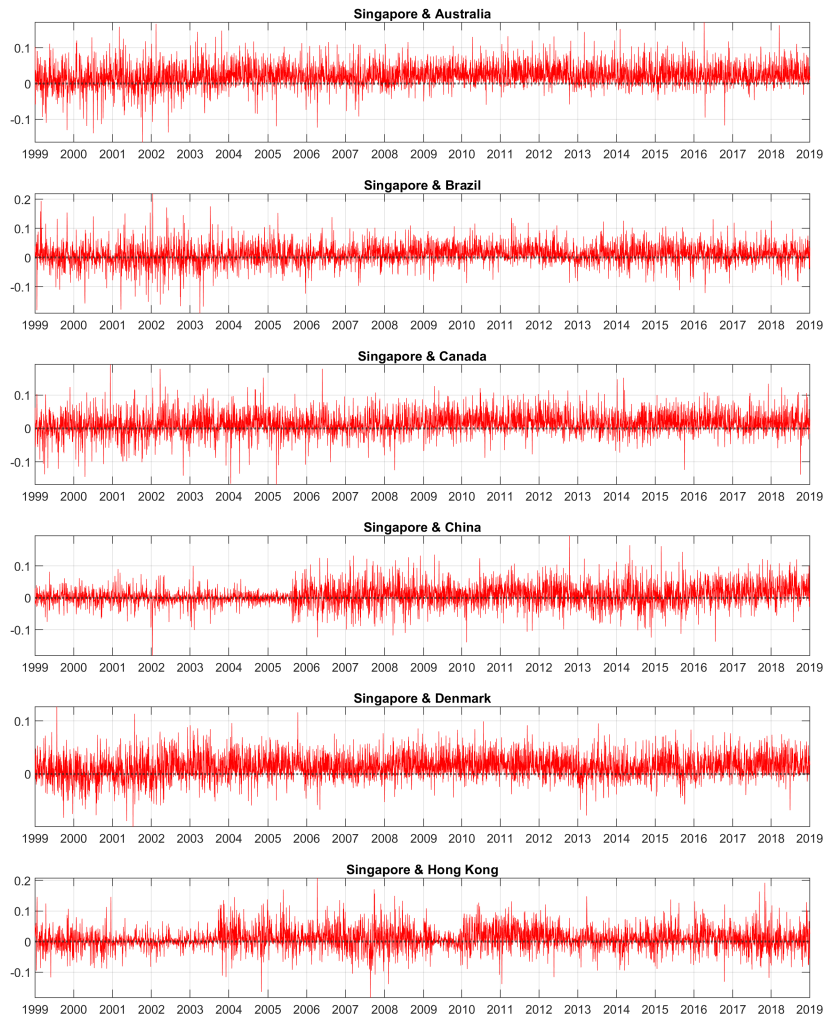


Figure A7: Dynamic Conditional Partial Correlations in Foreign Exchange Rate Volatility: A Comparative Analysis with Singapore 1

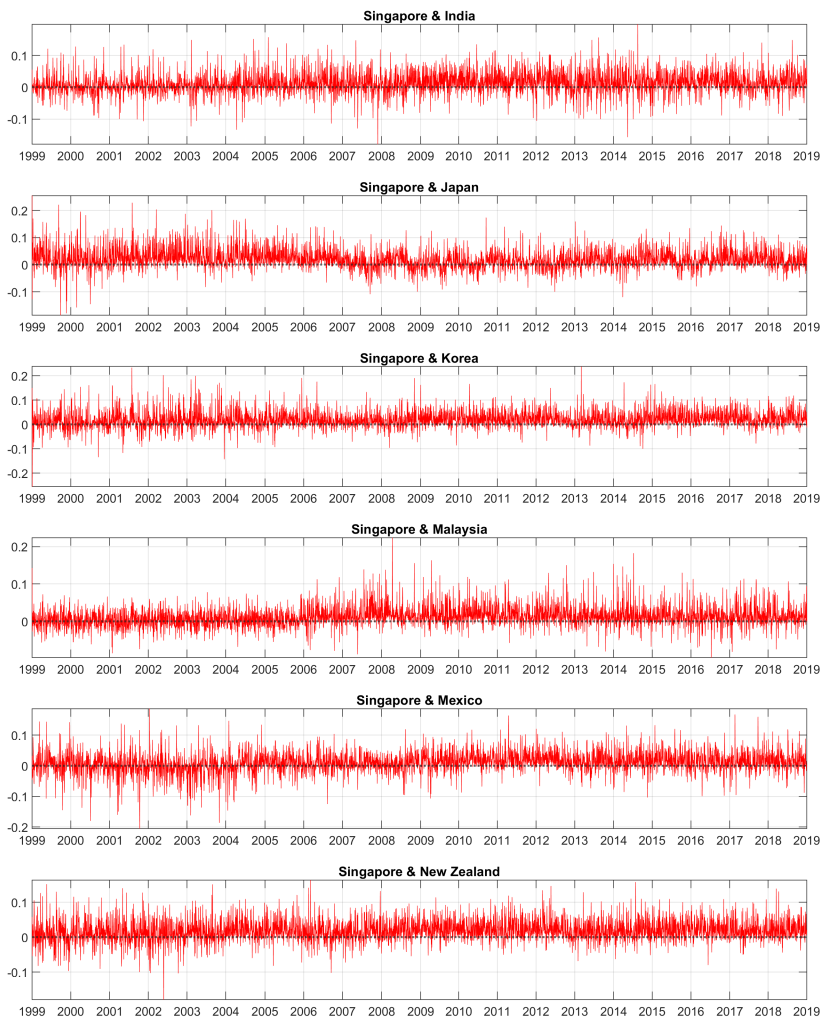


Figure A8: Dynamic Conditional Partial Correlations in Foreign Exchange Rate Volatility: A Comparative Analysis with Singapore 2

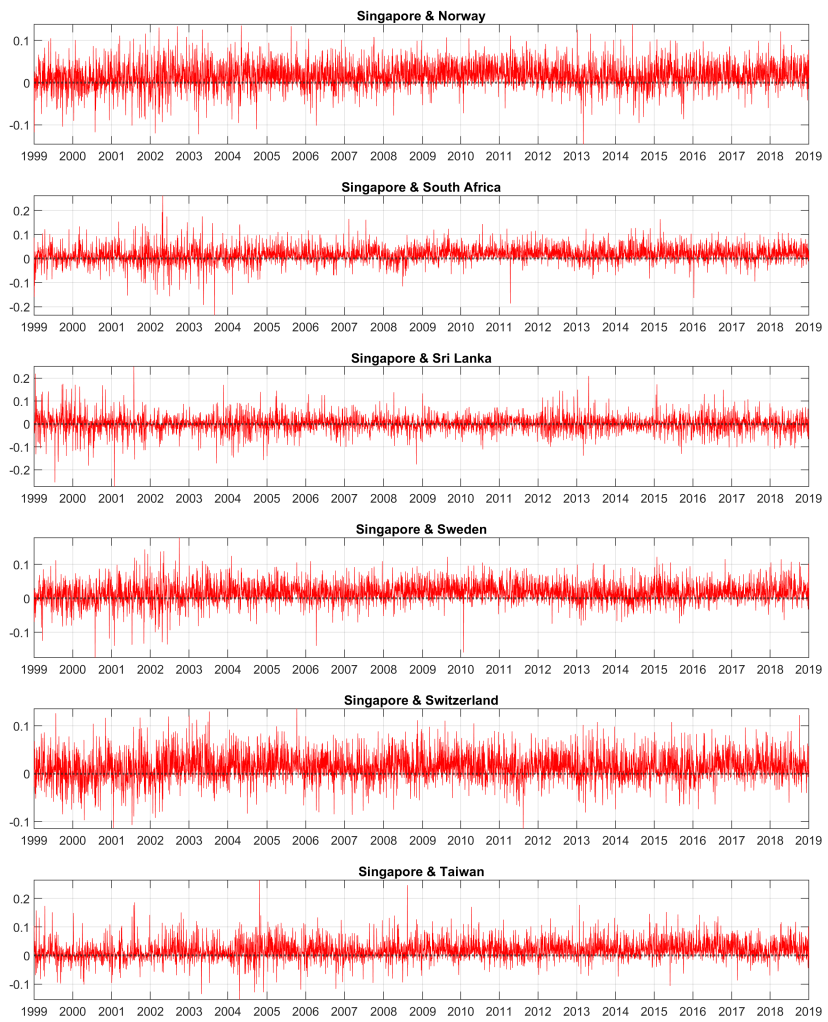


Figure A9: Dynamic Conditional Partial Correlations in Foreign Exchange Rate Volatility: A Comparative Analysis with Singapore 3

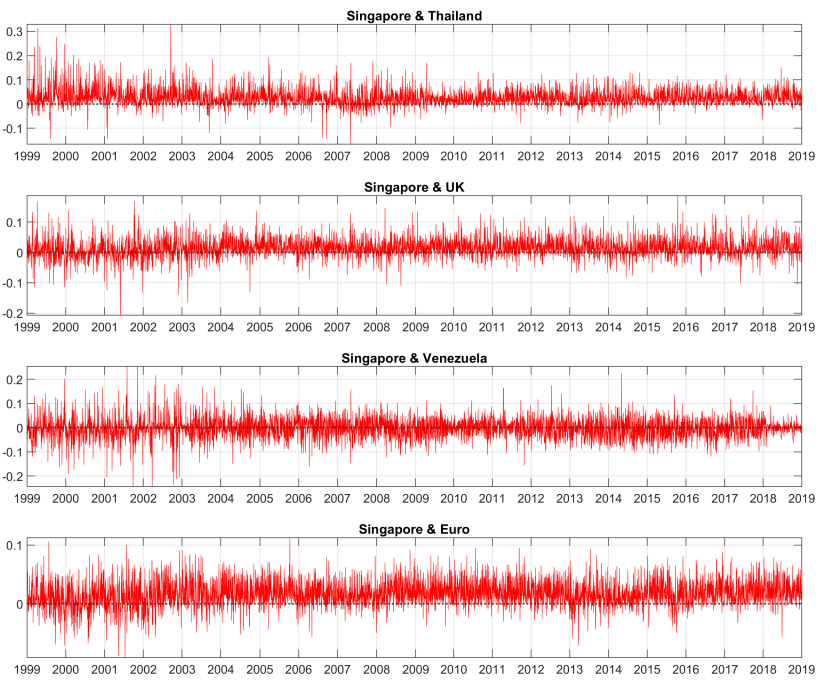


Figure A10: Dynamic Conditional Partial Correlations in Foreign Exchange Rate Volatility: A Comparative Analysis with Singapore 4

C List of Companies

Table A1 enumerates the corporations incorporated into the empirical analysis pertaining to the S&P 100 companies.

Table A1: List of Companies

Ticker	Company	GICS (Sector)	Ticker	Company	GICS (Sector)
AAPL	Apple Inc.	Information Technology	IBM	International Bus. Machines	Information Technology
ABBV	Abbvie	Health Care	INTC	Intel Corp.	Information Technology
ABT	Abbott Laboratories	Health Care	INTU	Intuit Inc.	Information Technology
ACN	Accenture plc	Information Technology	ISRG	Intuitive Surgical, Inc.	Health Care
ADBE	Adobe Inc.	Information Technology	JNJ	Johnson & Johnson	Health Care
AEP	American Electric Power	Utilities	JPM	JPMorgan Chase & Co.	Financials
AIG	American International Group	Financials	KO	The Coca Cola Company	Consumer Staples
ALL	Allstate Corp	Financials	LLY	Lilly (Eli) & Co.	Health Care
AMGN	Amgen Inc.	Health Care	LMT	Lockheed Martin Corp.	Industrials
AMZN	Amazon.com Inc.	Consumer Discretionary	LOW	Lowe's Cos.	Consumer Discretionary
APA	Apache Corporation	Energy	MCD	McDonalds Corp.	Consumer Discretionary
AXP	American Express Co.	Financials	MDLZ	Mondelez International	Consumer Staples
BA	Boeing Company	Industrials	MDT	Medtronic Inc.	Health Care
BAC	Bank of America Corp	Financials	MET	MetLife Inc.	Financials
BAX	Baxter International Inc.	Health Care	METTA	Meta Platforms Inc.	Information Technology
BK	The Bank of New York Mellon Corp.	Financials	MMM	3M Company	Industrials
BMY	Bristol-Myers Squibb	Health Care	MO	Altria Group Inc.	Materials
C	Citigroup Inc.	Financials	MRK	Merck & Co.	Health Care
CAT	Caterpillar Inc.	Industrials	MS	Morgan Stanley	Financials
CL	Colgate-Palmolive	Consumer Staples	MSFT	Microsoft Corp.	Information Technology
CMCSA	Comcast Corp.	Consumer Discretionary	NEE	NextEra Energy Inc.	Utilities
CME	CME Group Inc.	Financials	NFLX	Netflix Inc.	Communication Services
COF	Capital One Financial	Financials	NKE	NIKE Inc.	Consumer Discretionary
COP	ConocoPhillips	Energy	NOV	National Oilwell Varco Inc.	Energy
COST	Costco Co.	Consumer Staples	NSC	Norfolk Southern Corp.	Industrials
CRM	Salesforce Inc.	Information Technology	ORCL	Oracle Corp.	Information Technology
CSCO	Cisco Systems	Information Technology	OXY	Occidental Petroleum	Energy
CVS	CVS Caremark Corp.	Consumer Staples	PEP	PepsiCo Inc.	Consumer Staples
CVX	Chevron Corp.	Energy	PFE	Fisher Inc.	Health Care
DD	Du Pont (E.I.)	Materials	PG	Procter & Gamble	Consumer Staples
DELL	Dell Technologies Inc.	Information Technology	PM	Philip Morris International	Consumer Staples
DIS	The Walt Disney Company	Consumer Discretionary	QCOM	QUALCOMM Inc.	Information Technology
DVN	Devon Energy Corp.	Energy	RTN	Raytheon Co.	Industrials
EBAY	eBay Inc.	Information Technology	SBUX	Starbucks Corp.	Consumer Discretionary
EMR	Emerson Electric	Industrials	SUB	Schlumberger Ltd.	Energy
EXC	Exelon Corp.	Utilities	SO	Southern Co.	Utilities
F	Ford Motor	Consumer Discretionary	SPG	Simon Property Group Inc	Financials
FCX	Freight-McMoran Cp & Gld	Materials	T	AT&T Inc.	Communication Services
FDX	FedEx Corporation	Industrials	TGT	Target Corp.	Consumer Discretionary
GD	General Dynamics	Industrials	TXN	Texas Instruments	Information Technology
GE	General Electric	Industrials	UNH	United Health Group Inc.	Health Care
GILD	Gilead Sciences	Health Care	UNP	Union Pacific	Industrials
GM	General Motors	Consumer Discretionary	UPS	United Parcel Service	Industrials
GOOG	Google Inc.	Information Technology	USB	U.S. Bancorp	Financials
GS	Goldman Sachs Group	Financials	V	Visa Inc.	Information Technology
HAL	Halliburton Co.	Energy	VZ	Verizon Communications	Information Technology
HD	Home Depot	Consumer Discretionary	WFC	Wells Fargo	Financials
HON	Honeywell Int'l Inc.	Industrials	WMT	Wal-Mart Stores	Consumer Staples
HPQ	Hewlett-Packard	Information Technology	XOM	Exxon Mobil Corp.	Energy